Deep–Sea Research I 186 (2022) 103811

Contents lists available at ScienceDirect

Deep-Sea Research Part I

journal homepage: www.elsevier.com/locate/dsri

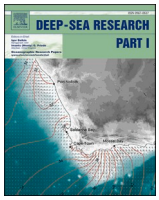

Benthic megafauna habitats, community structure and environmental drivers at Rio Grande Rise (SW Atlantic)

Paulo Vinicius Ferraz Corrêa [a,*], Luigi Jovane [a], Bramley J. Murton [b], Paulo Yukio Gomes Sumida [a]

[a] Instituto Oceanográfico da Universidade de São Paulo, São Paulo, Brazil
[b] National Oceanography Centre, Southampton, UK

ARTICLE INFO

Keywords:
Biodiversity
Geomorphology
Fe–Mn crusts
Deep-sea mining
Rio Grande rise
SW Atlantic

ABSTRACT

The Rio Grande Rise (RGR) is a large and geomorphologically complex feature located in the Southwest Atlantic, with great commercial and scientific interest due to its potential for mining rare earth elements that are critical for low-carbon technologies. Brazilian interest in this area led to the submission of a petition to the UN Commission on the Limits of the Continental Shelf in 2018 to include RGR on the limits of its continental shelf beyond 200 nautical miles. However, mining activities are potentially harmful to deep-sea ecosystems and will likely cause some extent of biodiversity loss. Thus, baseline and continuous environmental studies in the RGR are important to address potential conflicts between mineral extraction and the conservation of deep-sea biodiversity. The RGR is characterized by a series of summit plateaus of ~600 m deep divided NE-SW by a rift valley, up to 2000 m deep. In 2018, the plateaus and rift of a small area in RGR (30°35′S – 31°03′S, 35°36′W – 36°16′W) were explored through 13 dives of the robotic underwater vehicle (RUV) *HyBIS*. Videos were analyzed for the description of structuring factors (topography and habitat types) and to record benthic megafauna occurrences. Video transects revealed highly heterogeneous and rapidly changing habitats. Eleven habitats, five in the rift and six in the plateaus are proposed based on geomorphology, slope, and substrate textures. We recorded 17,008 megabenthic organisms classified in 83 morphotypes and six different phyla, from which Porifera (42.7%) and Cnidaria (41.5%) were the most representative. Samples were characterized by a high dominance and the dissimilarities result chiefly from differences in abundance scores. PERMANOVA tests indicated that Habitat and Region variables were the most important to explain structure within the community data, followed by depth and slope. The rift floor exhibited a low abundance of megabenthic epifauna, except in a sinkhole in the northern part of the rift. The lower and upper rift wall were characterized by different communities delimited by the transition between the Antarctic Intermediate Water and the Upper Circumpolar Deep Water. The habitats formed by Fe–Mn deposits were dominated by distinct communities, which were rarely observed elsewhere. Additionally, we found variations in community structure at regional scales (20–30 km), with distinct communities on each side of the rift and at the southwest of the study area. Our results contribute toward understanding the diversity, biogeography, and environmental drivers of the RGR. Fauna distribution is patchy, linked to habitats with potential mining resources, and dominated by Vulnerable Marine Ecosystems (VMEs) indicator taxa. Extensive community analysis should occur at a given site prior to consideration for the exploitation of natural resources.

1. Introduction

The deep sea is the largest environment on the planet, the ocean floor representing 63% of its entire area (Thurber et al., 2014) with a large potential for living and non-living resources (Herzig and Hannington, 1995). It exhibits one of the highest biodiversities of the planet (Mora et al., 2011; Ramirez-Llodra et al., 2010), much of it related to the heterogeneity of habitats, such as seamounts, continental margins, abyssal plains, ocean trenches, and particularly "extreme" physical-chemical environments such as hydrothermal vents and cold seeps. However, there are various challenges to study the deep sea, including those related to the high costs and complex logistics involved

* Corresponding author.
E-mail address: correapvf@usp.br (P.V.F. Corrêa).

https://doi.org/10.1016/j.dsr.2022.103811
Received 24 February 2022; Received in revised form 30 May 2022; Accepted 31 May 2022
Available online 3 June 2022

in expeditions. Therefore, there are large extensions of deep seafloor that are still little known to science, including important gaps in its biodiversity and ecology (McClain and Hardy, 2010; Perez et al., 2012).

Interest in deep-sea benthic environments has increased mainly owing to the search for commodities such as oil and gas, seafood, and high-tech minerals (Glover and Smith, 2003). The latter include rare-earth elements which are used in various applications, such as the manufacture of batteries, wind turbines, and solar panels (Hein and Koschinsky, 2014). Thus, there is a growing demand in the market for the consumption of these elements (Thompson et al., 2018). Deep-sea mining is a potential multibillion-dollar industry, expected to become operational in all the world's oceans within the next few decades, and it will invariably induce pressures in these uncharted environments (Hein and Koschinsky, 2014; Manceau et al., 2014).

In this scenario, the Rio Grande Rise (RGR) has gained special attention of researchers and governments around the world due to its mining potential for ferromanganese crusts (Fe–Mn). RGR is an extensive seamount region located between Brazil and Argentine basins (Cavalcanti et al., 2015) with origin commonly associated with an intense basalt spill in the Tristan da Cunha mantle plume (South Mid-Atlantic Ridge) about 75 million years ago. This event also gave rise to Walvis Ridge on the eastern side of the South Atlantic (Montserrat et al., 2019; O'Connor and Duncan, 1990). However, this hypothesis has been re-examined recently (Alberoni et al., 2020; Constantino et al., 2017; Graça et al., 2019). Most of the knowledge about RGR geology was collected during the *Deep-Sea Drilling Project* (DSDP) in the mid-1980s (Baker, 1983) and just in the last ten years, more expeditions were made in this area. The genesis of Fe–Mn crust deposits is still being discussed (Benites et al., 2020, 2021; Mohriak et al., 2010; Ussami et al., 2013).

The Brazilian government has a particular interest in this region. In 2015, the International Seabed Authority (ISA) and the state-owned Geological Survey of Brazil (CPRM) signed a 15-year contract for the exploration of 3000 km^2 in RGR (ISA, 2014; Montserrat et al., 2019). In 2018, the Brazilian government submitted its petition to the UN Commission on the Limits of the Continental Shelf (CLCS) to incorporate the RGR to the limits of its continental shelf beyond 200 nautical miles (LEPLAC, 2018). CLCS recommendations are thought to occur within the next few years and, if approved, RGR would be incorporated into Brazil's Economic Exclusive Zone.

Mining activities are potentially harmful to deep-sea ecosystems and will very likely cause some extent of biodiversity loss (Miller et al., 2018; Montserrat et al., 2019; Van Dover et al., 2017). Impacts include the direct removal of Fe–Mn crusts, increased sediment loads caused by mining tailings, release of wastewater at the sea surface (Hughes et al., 2015), and disturbance by noise. Given the lack of knowledge and species distribution data in the area, these activities may result in the removal of potentially undescribed species and the full impact of mining will be unknown. Hence, a baseline and continuous environmental studies on the sites and their surrounding areas before and during mining activities are important (Dunn et al., 2018). Data on fauna and community structure are essential so that mining activities remain sustainable and guarantee the protection of the deep-sea environment (Baker and Beaudoin, 2013). Valuable information about the vulnerability of habitats in the deep sea will provide supporting evidence to the creation of marine protected areas (Wedding et al., 2013) that will safeguard biodiversity and ecosystem function near mining sites (Guilhon et al., 2021).

At present, there are only fragmented biological data on RGR (Perez et al., 2012) that include fish records produced by Russian exploratory fishing from 1974 to 1988–1989 (Clark et al., 2007; Perez et al., 2012) and data from OBIS and GBIF databases (Montserrat et al., 2019). Recently, accounts on sponge gardens, dominated by the hexactinellid *Sarostegia oculata* (Hajdu et al., 2017), and benthopelagic fauna, limited to fishes and crustaceans (Perez et al., 2018) came to our knowledge. Demersal and longline fishing are also known to occur in the region (Morato et al., 2016), including the pelagic blue shark (Prionace glauca) and swordfish (Xiphias gladius) (Mourato et al., 2011) and the demersal alfonsino (Berix splendens) (Perez et al., 2012), representing additional human uses that may be compromised by deep-sea mining. Therefore, studying the biodiversity and understanding the ecological patterns of RGR communities are imperative during the following years to mitigate human impacts and better preserve this unique ecosystem.

2. Material and methods

2.1. Study area

The Rio Grande Rise is a complex positive feature located between the Argentine and Brazilian abyssal basins (28°S – 35°S; 28°W – 39°W), approximately 1200 km off the Brazilian coast and 2000 km off the Mid-Atlantic Ridge (Montserrat et al., 2019). It corresponds to the largest submarine elevation in southeastern Brazil (~480,000 km^2), rising from depths of 5000 m to peaks less than 600 m (Mohriak, 2020). RGR is usually divided into two sub-regions (Fig. 1a): (1) the Western Rio Grande Rise (WRGR) is characterized by a large ellipsoidal bulge that rises to a mean depth of about 2000 m and (2) the Eastern Rio Grande Rise (ERGR) with a north-south elongated geomorphology, delimited by E-W fractures in both north and south ends. There is a characteristic NW-SE rift structure formed on top of the bathymetric high (sometimes also referred to as 'graben' in the literature), creating a deep submarine channel, also called Cruzeiro do Sul rift.

The rift extends along the center of WRGR to the southern of the ERGR (Fig. 1a). It provides an extremely steep slope up to the rim of the RGR plateaus, where Fe–Mn crusts are more common (Montserrat et al., 2019). Due to the large size of RGR, sampling was focused in a small area in the middle of WRGR, between latitudes 30°35′S – 31°03′S and longitudes 35°36′W – 36°16′W (Fig. 1b). The rift bottom in the study area is up to 1500 m deep and 22–33 km wide. On both sides of the rift there are plateaus, ranging from 600 to 700 m depth, that extends beyond the study area.

Three water masses are found in the study region: the South Atlantic Central Water (SACW), the Antarctic Intermediate Water (AAIW), and the Upper Circumpolar Deep Water (UCDW) (da Silveira et al., 2020; Jovane et al., 2019; Peterson and Whitworth, 1989; Stramma and England, 1999). The shallowest portion of the studied area (ca. 100–600 m depth) is bathed by the SACW, which originates in the South Atlantic Subtropical Gyre, characterized by a local oxygen minimum (~4.7 mL/L O_2). Below the SACW, the AAIW is present, being characterized by a minimum salinity and maximum oxygen (~5.1 mL/L O_2) at around 800–900 m. AAIW, originating from the Subantarctic Front, is considered nutrient-rich and it ranges from 600 to 1100 m depth. The UCDW originates between the Subantarctic and the Polar Fronts and it is identified by a second local oxygen minimum (~4.2 mL/L O_2) together with a silicate maximum, ranging approximately from 1100 m to 1600 m depth.

2.2. Data collection

Data was collected during the DY094 expedition of the *RRS Discovery* (National Oceanography Centre, Southampton, UK) as part of the FAPESP/RCUK funded project Marine E-Tech, from October 26 to November 8, 2018. The expedition included 13 dives of the Robotic Underwater Vehicle, *RUV HyBIS* (Murton et al., 2012), used to collect physical samples and video footage of the seafloor (Fig. 1b–g). *HyBIS* was equipped with a Sony Full HD camera that recorded over 36 h and 26 km of the seabed (Table 1) and a robotic arm used to collect 10 voucher specimens from the most abundant representatives found during the survey. *HyBIS* was connected to the ship USBL system to record its position (latitude, longitude, and depth). Multibeam echosounder and backscatter data were acquired using a ship-mounted Kongsberg EM122. Multibeam processing was done using Caris HIPS and SIPS

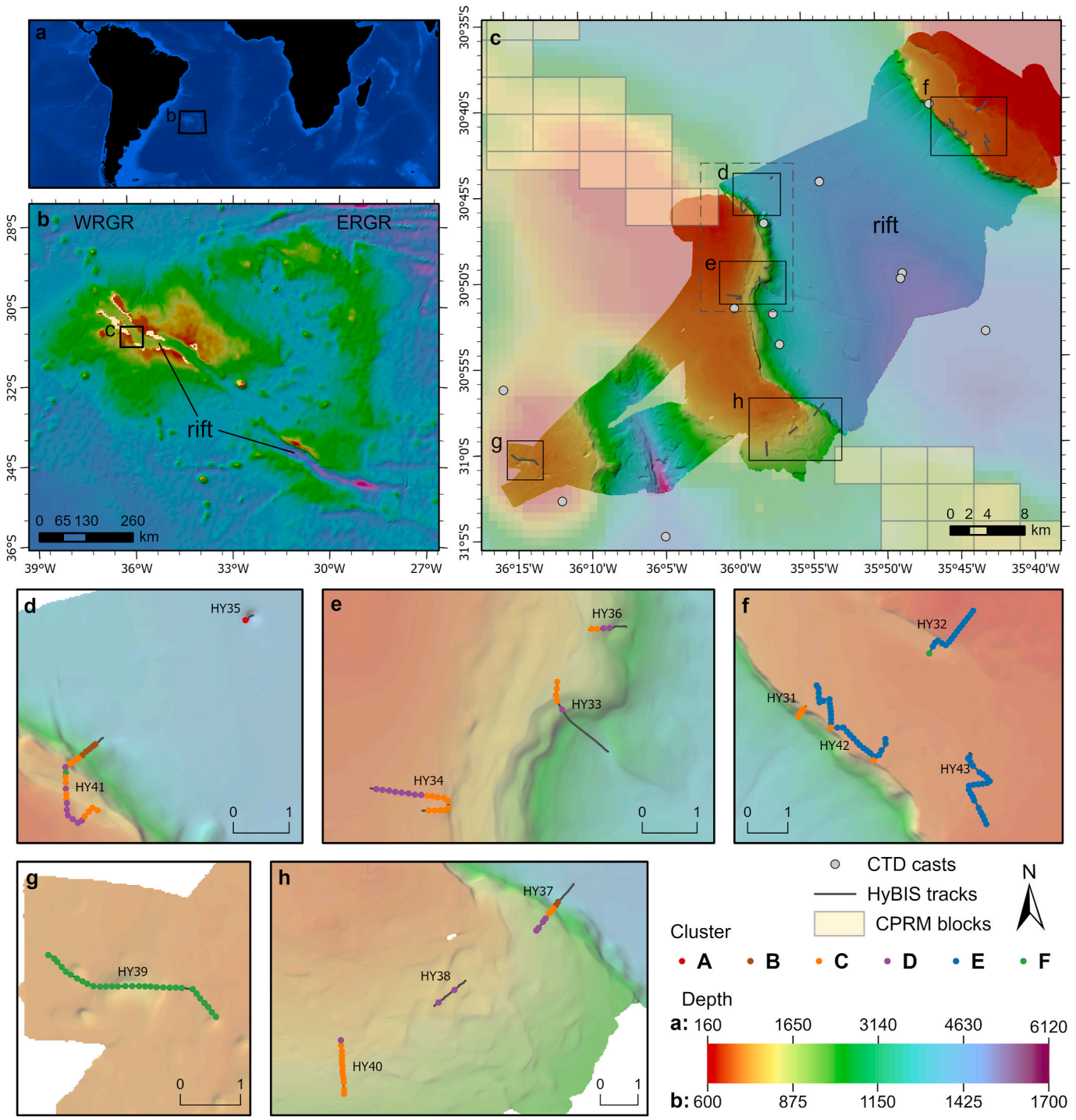

Fig. 1. **(a)** General South Atlantic view and area where the Rio Grande Rise is located. **(b)** Rio Grande Rise, South Atlantic. WRGR - Western Rio Grande Rise and ERGR - Eastern Rio Grande Rise. **(c)** Study area and bathymetry data acquired during the DY094 expedition in the RSS Discovery, and CTD casts made during the N/Oc. Alpha Crucis *expedition, 2018*. Black rectangles represent the extent area of the panel with its corresponding letter. Yellow rectangles represent the exploration area agreed in the contract between ISA and CPRM. **(d–h)** *HyBIS* dives (HY– codes) from the DY094 expedition. Greyed lines are the RUV tracks and each dot is a 120 m long segment extracted from the track. Dot colors represent clusters in which the segment was assigned (see results). Scales are in kilometers. **(d, e).** Center region. **(f)** Northeast region. **(g)** Southwest region. **(h)** South region.

v9.1.8 and the data were gridded at 15 m. Backscatter processing was done with FM Geocoder Toolbox v7.8.3 and the data were gridded at 5 m.

A set of additional seafloor variables was derived from the bathymetric data using the Benthic Terrain Model 3.0 tool (Walbridge et al., 2018) in ArcGIS 10.8. These variables were Slope, Aspect (measured in terms of northness and eastness), Roughness (11 neighborhood size), curvature, fine-scale (3/30 radius) Bathymetric Position Index (BPI), and broad-scale (20/200 radius) BPI. Neighborhood size and radius were chosen to minimize correlation between variables.

HyBIS videos were analyzed in two steps. Firstly, we annotated seafloor characteristics according to geomorphology, slope, and substrate textures following the classification system proposed by Greene et al. (2007, 1999), similar to the classification made by (Perez et al.,

Table 1
Benthic habitats observed during the *HyBIS* survey in the DY094 cruise in Rio Grande Rise (SW Atlantic). See Table 2 for a description of each habitat and Fig. 2 for a visual reference of each region. "Moving ahead time" ignores time spent when *HyBIS* was stopped collecting samples or performing system checks. Note that number of segments, time, distance, and number of records were pooled for habitat and region. Number of segments refers only to continuous segments above the threshold of 96 m long (80% of 120 m, see results below) and 20 records.

Habitat	Region	Dives	No. segments	Moving ahead time	Distance (m)	No. records
Rift Coral Debris (RiftDeb)	Center	33, 41	0	00:40:32	443.9	29
	South	37	0	00:52:31	574.1	29
Rift Floor Sediment (RiftSed)	Center	33, 35	0	01:10:05	840.1	43
	South	37	0	00:14:02	127.3	31
Rift Sinkhole (RiftHole)	Center	35	1	00:35:56	167.7	154
Rift Wall (RiftRock)	Center	33, 36, 41	18	03:42:41	2494.5	1171
	South	37	2	00:34:31	437.7	96
Rift Wall Crusts (RiftCr)	Center	34, 36, 41	7	01:04:30	871.8	1414
	Northeast	31	5	00:49:32	584.2	1268
	South	37	3	00:24:51	331.9	351
Sediment (Sed)	Northeast	32, 42, 43	11	02:43:38	1792.1	429
	Southwest	39	5	00:43:49	631.5	408
Calcarenite Pavement (CalPav)	Center	34, 41	18	02:59:10	2184.7	1026
	Northeast	32	1	00:07:30	124.8	60
	South	37, 38	6	02:28:46	1722	350
	Southwest	39	26	03:18:13	2821.5	4589
Crust Pavement (CrPav)	Center	33, 34	10	01:26:52	1206.8	1246
	Northeast	31, 42, 43	14	02:53:53	1921.6	624
Crust Sediment (CrSed)	Northeast	42	28	04:44:20	3361.2	1177
	South	40	13	02:18:01	1690.7	1261
Crust (Cr)	Northeast	32	10	01:24:25	1107	915
Crust Cobble (CrCob)	Northeast	32	5	00:50:59	583.9	306
	Southwest	39	0	00:03:10	50.6	31
Total			**183**	**36:11:57**	**26,071.6**	**17,008**

2018) on adjacent areas in RGR. Habitats, observed along with the RUV dive, were defined based on a unique combination of these features. Habitats were classified in three spatial scales: (1) 'Subsystem' (tens of kilometers to a kilometer), (2) 'Class' (a kilometer to tens of meters), and (3) 'Subclass' (one to tens of meters). We only considered a transition from one habitat to another when their features changed abruptly (~10 s) and remained changed for at least 30 s. Secondly, we annotated and counted the benthic fauna directly from videos in a macro-enabled Microsoft Excel file, which supports reading timestamp from the video player and opening a video in at any specific annotation. Records were classified in the lowest possible taxonomic group and identified to morphotypes based on morphological features observed in the images, except for cases where identification to the species level was possible. Highly motile fish and crustaceans were noted but not included here, as distinct drivers may affect this fauna and will be subject of future studies. Observations and morphotypes classification were double checked to ensure consistency in the video annotations. Voucher specimens were collected to improve identification of morphotypes. We assigned a unique code for each morphotype/species, composed of four letters and one number. The number of records from the videos was used as abundance and the count of morphotypes as species richness.

In addition, data from a previous expedition to RGR on board the N/Oc. Alpha Crucis *in February 2018, also as part of the Marine E-Tech Project, were used. During this cruise, 13 CTD casts* (stations 468–497, see Jovane et al., 2019 for details) *were made in the study area to record water column properties, namely Temperature (°C), Salinity (PSU), and Oxygen (mg/L). Each cast was averaged in 10 m depth bins and calculated by draping the RUV depth in each bin and interpolating using the IDW function of the* gstat *package* (Gräler et al., 2016) *in R.*

2.3. Data analysis

All statistical analyses were performed in R, version 4.0.3 (R Core Team, 2020), and package *vegan* for community and multivariate analysis (Oksanen et al., 2019). Permutation tests were made using 9999 permutations and a restricted permutation of type series within each dive to account for dependence of the data. Graphs were made using the *ggplot2* package (Wickham, 2016).

HyBIS tracks were divided in segments (samples) to conduct quantitative analysis. These segments followed the previously defined habitat delimitation to assure that no segment would cover two distinct habitats. Segments were allowed to vary down to 80% of the segment size to ensure the track was covered by the segments as much as possible. Segments with lower than 20 faunal observations were removed from further analysis as they bear little information about the community in these areas. Multiple threshold lengths for the segments were tested and we chose the one that accounts for the most abundance overall. Smaller values generate more fragmented segments with lower abundance and more segments are discarded for not having a minimal 20 observations. On the other hand, larger values generate fewer longer segments, but more regions are discarded for not having the minimal length required.

We grouped *HyBIS* dives based on the region within the study area they were made (Fig. 1). "Northeast" as dives HY31, HY32, HY42, and HY43 on the northern side of the rift; "Center" as dives HY33, HY34, HY35, HY36, and HY41 on the west side of the rift; "South" with dives HY37, HY38, and HY40 in the south of the rift; and "Southwest" as the single dive HY39 in the southwest extreme of the study area.

We plotted species accumulation curves and richness estimators with samples randomized 1000 times to analyze the overall diversity that was detected in the videos, namely Chao1, First-order jackknife, ACE, and Bootstrap (Magurran, 2004). Community data was log-transformed using R function *log1p* to decrease the influence of abundant species. Then, we calculated Bray-Curtis dissimilarities (also referred as percentage difference) to compare changes in communities along with samples. We used Unweighted Pair Grouping Method with Arithmetic Mean (UPGMA) clustering to identify segments with similar community structures within the study area. Fusion levels and silhouette plots were used to identify the optimal number of clusters, following the methods described by Borcard et al. (2018). The obtained community clusters were validated by using non-metric Multidimensional Scaling (nMDS) ordination technique, which makes a 2-dimension representation of morphotype composition similarities among all samples.

The identified clusters were then characterized based on their most abundant taxa and Indicator Value indices (IndVal) (Dufrêne and Legendre, 1997). The IndVal method is aimed to compare the association between species patterns and combinations of groups of sites and

identify species that can be used to discriminate a group of samples from all other samples in the analysis. The Multilevel pattern analysis was carried out with the *indicspecies* package (Cáceres and Legendre, 2009) using IndVal as a function with a correction for clusters with different sizes. Furthermore, clusters were characterized based on the regions and habitats they were more predominant and by using univariate diversity measures, mean abundance, richness (S), Shannon index ($H'_{\log e}$), and Pielou's evenness (J) (Pielou, 1966). We used a chi-square test to check a significant association between the clustering typology to distinct regions and habitats.

Collinearity between environment linear variables (derived from multibeam data plus CTD casts) was checked using Pearson's rank correlation coefficient and variables with a high correlation (>0.7) were removed from further analysis. Effects of habitat, region, and linear variables in the community data were tested with PERMANOVA (Anderson, 2001; McArdle and Anderson, 2001) using the *adonis2* function with terms added sequentially. We used the PERMDISP2 (Anderson, 2006) to verify the homogeneity of dispersions of habitat

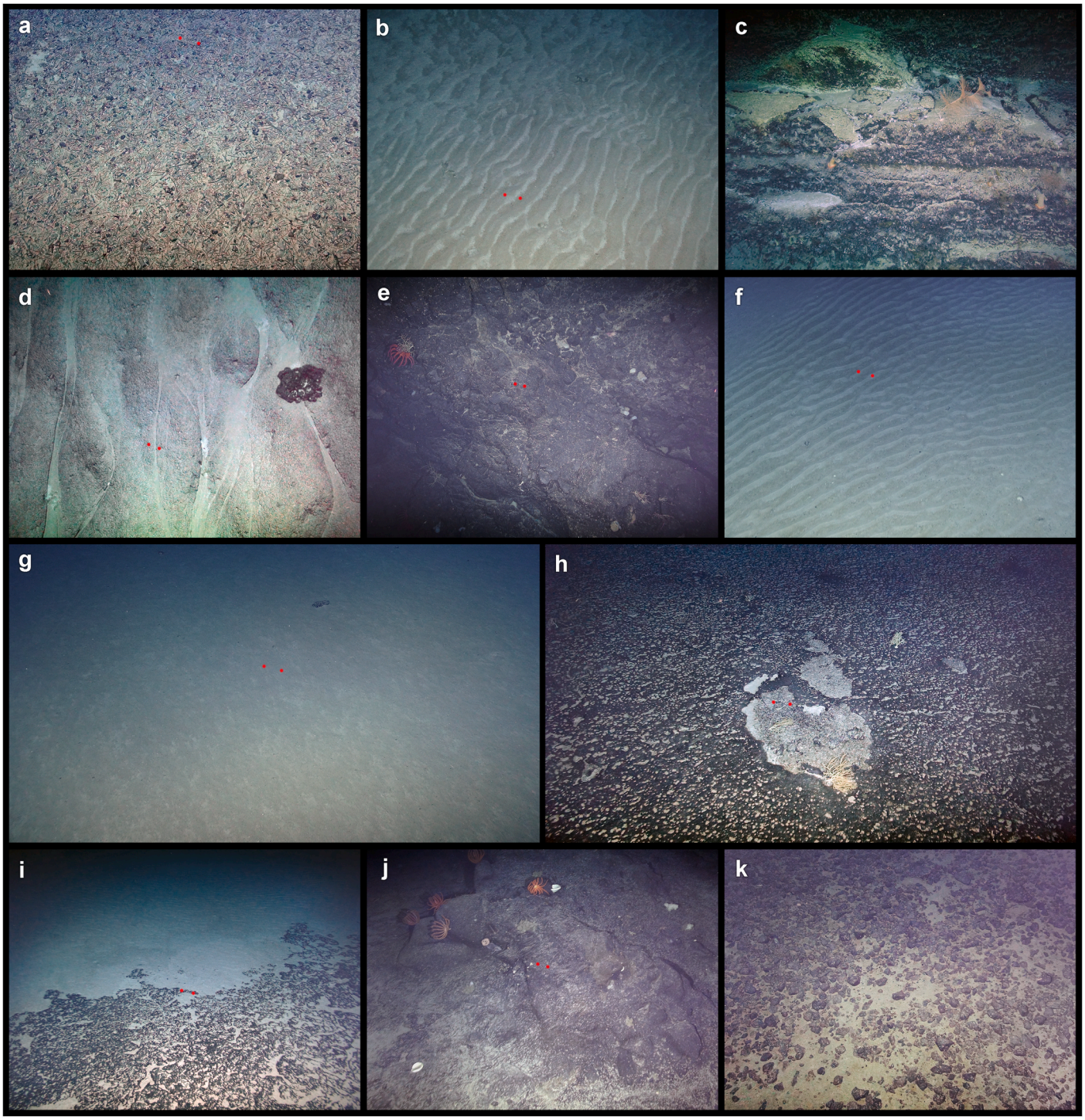

Fig. 2. Benthic habitats observed in Rio Grande Rise (SW Atlantic). **(a)** Rift Coral Debris (RiftDeb), HY33. **(b)** Rift Floor Sediment (RiftSed), HY33. **(c)** Rift Sinkhole (RiftHole), HY35. **(d)** Rift Wall (RiftRock), HY33. **(e)** Rift Wall Crusts (RiftCr), HY41. **(f)** Sediment (Sed), HY43. **(g)** Calcarenite Pavement (CalPav), HY34. **(h)** Crust Pavement (CrPav), HY33. **(i)** Crust Sediment (CrSed), HY40. **(j)** Crust (Cr), HY32. **(k)** Crust Cobble (CrCob), HY32. Laser dots are 10 cm apart and visibility was manually enhanced, except in panels (c) and (k), where they were not visible.

and region groups, as otherwise, PERMANOVA can result in false detection of a difference of means. We made violin plots of the variables that significantly explained the variance in the community grouped by the clusters and used a non-parametric Kruskal-Wallis test (Kruskal and Wallis, 1952) and its corresponding post-hoc comparisons (with Holm correction) to compare the selected variables between the community clusters (Borcard et al., 2018). We previously used ANOVA, but the test failed its assumptions.

Finally, we carried out a Multivariate Regression Tree analysis (MRT) (De'ath, 2002). The method is an extension of Classification and Regression Tree analysis (CART) to multivariate data. It tries to identify discontinuities in the response data, e.g. community composition, and associate these discontinuities to specific values of the explanatory data, e.g. environmental data. The analysis was carried using the *mvpart* package (De'ath, 2002; Borcard et al., 2018), with Hellinger transformed abundance data, as other dissimilarities (e.g. Bray-Curtis) are not fully implemented in the method, and environment variables with significant effect in the PERMANOVA test. The optimal size of the tree (i.e., the number of leaves) was decided based on the Cross-Validation Relative Error (CVRE) closest to one standard error of the smallest CVRE value. Ten folds were used in cross-validation, repeated 100 times.

3. Results

3.1. Habitat classification

We observed 11 habitats during the *HyBIS* dives differentiated by depth, slope, and substrate type (Fig. 2, Table 1, and Table 2). Five were found in the rift and six on the plateaus. The rift floor was filled by soft sediment with Fe–Mn coated pieces of corals (mostly Isididae) and cobbles on top (RiftDeb, Fig. 2a) or by pteropods shells and forams (RiftSed, Fig. 2b). The latter was found next to rift walls on dives HY33 and HY37, but not in dive HY41, in which RiftDeb was next to the rift wall. Both habitats had a smaller number of animal sightings when compared to other areas of RGR (Table 1). The northwest end of the rift featured a sinkhole, which was observed during the dive HY35. The bottom of the sinkhole was composed of soft sediments, like other areas of the rift, and its wall was composed of layered calcareous chalks

Table 2
Classification and description of benthic habitats observed in Rio Grande Rise (SW Atlantic). The classification system is in accordance with the scheme proposed by Greene et al. (1999), based on the DTM of the area and in-situ video data. Mean depth (m) and slope (°) are provided in round brackets in subsystem and subclass respectively. Values after semicolons are minimum and maximum, respectively.

Habitat	Subsystem	Class	Subclass	Modifiers
RiftDeb	Rift floor (1311.4; 1197–1396)	Debris Field	Sloping (13.8°) Sand with pebble and corals debris	Contiguous Fe–Mn coated coral (Isididae) debris on top of soft sediment Scattered Fe–Mn coated pebble
RiftSed	Rift floor (1250.0; 1021–1486)	Bedform, Sediment waves	Sloping (13.9°) Mixed sand and ooze	Undulated surface and Ripples (≈10 cm in amplitude), thick, semi to well consolidated Scattered thin deposition of pteropods shells and forams Occasional sparsely cobbles and coral debris Regular calcarenite pavement underlying
RiftHole	Rift floor (1449.0; 1419–1489)	Scarp Wall	Steeply Sloping (35.9°) Bedrock - Igneous	Wall of a sinkhole in the floor of the Rift Layered calcareous chalks Scattered deposition of sediment near the top of the hole
RiftRock	Rift wall (941.6; 708–1268)	Scarp Wall	Sloping to Steeply Sloping (21.2°) Bedrock - Igneous	Irregular volcanic outcrops (basalts) Scattered fractures Scattered thin deposition of sediment accumulated in cracks and crevices Occasional boulders or Fe–Mn crusts debris
RiftCr	Rift wall (882.3; 709–1114)	Scarp Wall	Steeply Sloping (38.8°) Bedrock - Fe–Mn crust	Irregular Fe–Mn crust or Fe–Mn coated outcrops Scattered thin deposition of sediment accumulated in cracks and crevices Patchy distribution of *Sarostegia oculata*
Sed	Plateaus (701.5; 668–810)	Bedform, Sediment waves	Flat (2.5°) Mixed sand and ooze	Undulated surface and Ripples (≈10 cm in amplitude), thick, semi to well consolidated Scattered thin deposition of pteropods shells and forams Occasional sparse cobbles Regular calcarenite pavement underlying
CalPav	Plateaus (751.9; 679–921)	Flat	Flat to Sloping (7.5°) Pavement - Calcarenite	Regular calcarenite pavement Occasional Fe–Mn coated boulders Dusting sediment cover Patchy distribution of black corals, sea urchins, and other suspension feeders
CrPav	Plateaus (707.4; 664–906)	Flat	Flat (5.3°) Pavement - Fe–Mn crust	Regular Fe–Mn crusts pavement Scattered dusting or thin sediment cover Occasional step-like structures (<1m in height), with calcarenite on bottom and Fe–Mn crusts on top Most likely target area for exploration Patchy distribution of *Sarostegia oculata*
CrSed	Plateaus (740.3; 687–865)	Flat	Flat to Sloping (2.2°) Mixed Fe–Mn crust Pavement and sand	Mixed Regular Fe–Mn crusts with calcarenite pavement, alternating every 5–10 m Often deposition of thin to thick sediment Scattered ripple marks on the sediment Fauna often fixed on Fe–Mn crusts
Cr	Plateaus (636.3; 627–688)	Exposure - outcrops	Flat to Sloping (3.8°) Bedrock - Fe–Mn crust	Irregular volcanic outcrops with Fe–Mn crust cover Scattered thin deposition of sediment Patchy distribution of sponges and brisingid seastars
CrCob	Plateaus (702.3; 688–746)	Flat	Flat to Sloping (3.6°) Fe–Mn cobble field	Contiguous Fe–Mn coated cobbles and small boulders (<60 cm) on top of regular calcarenite pavement and red clays Scattered deposition of thin to thick sediment cover

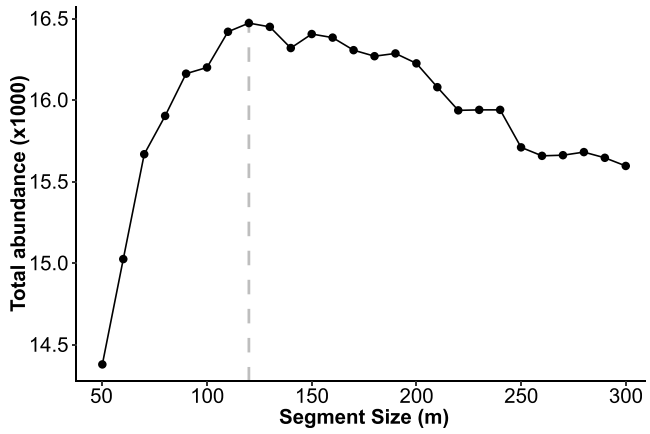

Fig. 3. Overall abundance accounted within the segments when using multiple threshold lengths to define the segments. The vertical dashed line indicates the value used in this work, 120 m.

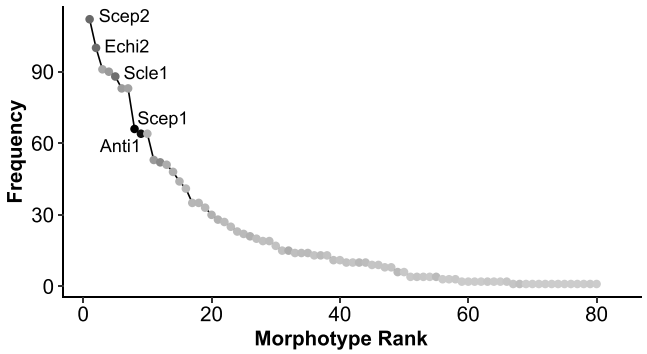

Fig. 4. Rank frequency diagram of the morphotypes observed by the *HyBIS* in Rio Grande Rise (SW Atlantic). The five most abundant taxa are labeled. Scep1 - *Sarostegia oculata*, Anti1 - *Aphanostichopathes* sp., Echi2 - *Gracilechinus* sp., Scep2 - *Aphrocallistes* cf. *beatrix*, and Scle1 - *Enallopsammia rostrata*. Darker colors indicate morphotypes with higher abundance.

(RiftHole, Fig. 2c). The rift wall on both sides was steep, varying from 30° to 60°, and was almost vertical at its upper half. Walls were mainly composed of exposed basaltic outcrops near the bottom (RiftRock, Fig. 2d) and irregular Fe–Mn crusts or Fe–Mn coated outcrops near the top of the rift (RiftCr, Fig. 2e). The transition from one substrate to another was not well defined and it occurred at multiple depths across dives. The plateaus were flat (0°–10°) with an abrupt chasm from the rift in most places.

The plateaus area was partially composed of soft sediment with conspicuous ripple marks, pteropods shells, and foraminiferal tests (Sed, Fig. 2f). However, three habitats were the most common during our survey (Table 1). One was composed of large pavements of carbonate rock and seemingly exposed to strong current flux (CalPav, Fig. 2g). The second is formed by large plate-like Fe–Mn crusts (CrPav, Fig. 2h). The third is composed of these two substrates, with plate-like crusts intermingled by calcarenite pavements and often with sediment pools (CrSed, Fig. 2i). During Dive HY32, we observed two more habitats that were almost exclusive of the northeast of the study area. Above the terrace at the northeast area of the dive was formed by irregular volcanic outcrops with Fe–Mn crust cover and a few sediment pools (Cr, Fig. 2j), similar to the substrate found in the RiftCr. The area below the terrace on dive HY32 and in a small segment of dive HY39 (which were not included in the analysis due to its small size) was composed of pavements of carbonate rock with fields of Fe–Mn coated cobbles and small boulders (CrCob, Fig. 2k). Outcrops with hardground rocks of volcanic and other origin have been recognized, but they were not long enough to be classified as a single habitat. Habitat classification and modifiers can be seen in Table 2. Habitats RiftSed, RiftRock, CalPav, Cr, Sed, and CrPav are respectively similar to GB, GW, SCA, SCR, SSD, and SCT in Perez et al. (2018).

3.2. Faunal community

We found 83 different morphotypes representing six different phyla (Suppl. data 1) and 17,008 records of megabenthic organisms. Porifera contributed 42.7% to the abundance; Cnidaria, 41.5%; Echinodermata, 12.9%; Mollusca, 0.3% and Arthropoda, 0.03%. Nineteen of these taxa were rare, i.e. represented by one or two individuals. The overall community was characterized by a great dominance of five morphotypes: the coral-mimicking hexactinellid sponge *Sarostegia oculata* Topsent, 1904 (Scep1) and its epibiont *Thoracactis topsenti* represented 29.3% of all individuals in this study, followed by the unbranched black coral *Aphanostichopathes* sp. (Anti1, 24.9%), the sea urchin *Gracilechinus* sp. (Echi2, 7.1%), the hexactinellid *Aphrocallistes* cf. *beatrix* Gray, 1858 (Scep2, 7.1%), and the scleractinian *Enallopsammia rostrata* (Pourtalès, 1878) (Scle1, 6.2%). These five taxa represent 74.6% of all abundance captured by the images.

The best length for segments that would maximize the number of faunal observations was 120 m (Fig. 3). Regression analysis showed this difference was not significant in comparison with abundance ($r = -0.552$, $p = 0.55$) and richness ($r = 0.005$, $p = 0.94$). *HyBIS* tracks were divided into 183 segments (Table 1) comprising 16,176 observations and 80 morphotypes total. The remaining 832 individuals and 3 morphotypes were from small habitat areas and were discarded from further analysis. The number of specimens observed in each segment varied largely from 20 to 492. Fifty-one segments had more than 100 records, 80 segments had less than 50 records, and 36 (not accounted for the 183 total) segments were discarded from ecological analysis due to the small number of individuals (<20). Most of these comprised the RiftRock, RiftSed, RiftDeb, and South-CalPav habitats.

Aphrocallistes cf. *beatrix* (Scep2) was the most frequent taxon and it was present in 112 segments, followed by *Gracilechinus* sp. (Echi2) which is present in 100 segments (Fig. 4). *Chaunax suttkusi* Caruso, 1989 (Loph1), Astrophorina (Desm1), *Enallopsammia rostrata* (Scle1), Brisingidae (Bris1), and *Helicolenus* sp. (Scor1) were present in more than 80 segments, but they had low abundance (<300 records) compared to the dominant taxa, with exception of *E. rostrata*. *Sarostegia oculata* (Scep1) and *Aphanostichopathes* sp. (Anti1) were the two most dominant taxa, and they had a frequency of 66 and 64%, respectively. Half of the morphotypes were found in 10 or fewer segments and a quarter was found in one or two segments. Morphotype accumulation curves show that all habitats did not reach the asymptote (Fig. 5a and b), especially for habitat 'RifHole' where only a small area was observed. Habitats 'RiftSed' and 'RiftDeb' had much smaller accumulation curves compared to the other habitats. Likewise, richness estimators did not reach the asymptote (Fig. 5c), except for Chao1. They estimate a richness from 85.6 to 93.9 for 183 segments.

The UPGMA clustering analysis identified six distinct community clusters (Fig. 6a). There are four main clusters (C, D, E, and F) that contained 175 segments out of 183. The Chi-squared test indicated a significant association of the clustering with different habitats ($x^2 = 461.7$, $p < 0.001$) and regions ($x^2 = 323.4$, $p < 0.001$). Fig. 6b shows a clear higher relative abundance of *S. oculata*, *Gracilechinus* sp., *Aphrocallistes* cf. *beatrix*, and *Aphanostichopathes* sp. in clusters C, D, E, and F respectively. Cluster A is composed of a single segment from the RiftHole habitat at the Center region (Figs. 1c and 7a). Cluster B consists of 7 segments in the west rift wall in both Center and South regions, near the rift floor (Fig. 1c, g), exclusively in the RiftRock habitat (Fig. 7b). Cluster C includes segments on both sides of the rift wall, in the plateaus near the rift wall, or the sloping area in the South region (Fig. 1c–e, g). This cluster was predominant in habitats with Fe–Mn crust substrate and it

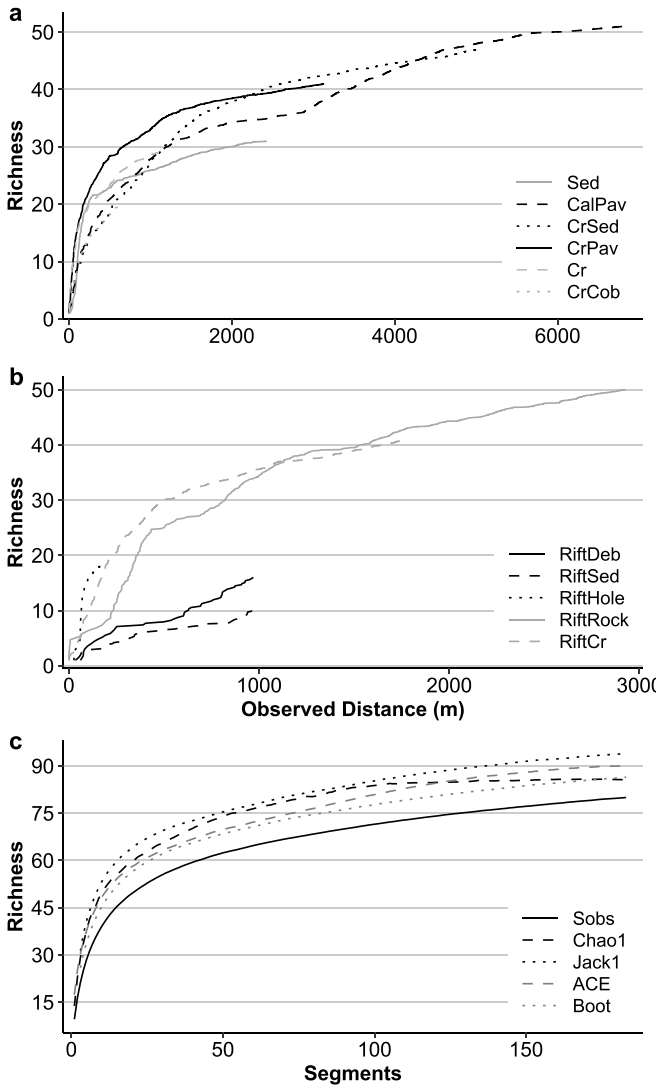

Fig. 5. Benthic randomized morphotypes accumulation curves in Rio Grande Rise (SW Atlantic). **(a, b)** Richness of each habitat based on the observed distance with the *HyBIS*. **(a)** Habitats in the plateaus. **(b)** Habitats in the rift. Note that X-axis scales are different in (a, b). **(c)** Overall observed accumulation curve (Sobs) and estimates (Chao1, Jakknife1, ACE, and Bootstrap) of morphotypes based on the number of segments.

has a few segments of RiftRock and CalPav as well (Fig. 7c). Cluster D comprises segments at the Center and South regions (Fig. 1c–d, g) and it was predominant in the habitat CalPav on the plateaus (Fig. 7d). Cluster E was the largest one with 66 segments and it was located exclusively in the Northeast region (Fig. 1c–d, g). It mostly occurred in habitats with Fe–Mn crust substrate as well (Fig. 7e). Cluster F consists of segments that completely cover the Southwest region and in dives HY32 and HY41 (Fig. 1c, e-f). This cluster was predominant in the CalPav habitat (Fig. 7f).

According to the Indicator Value indices (IndVal) and pattern analysis, Cluster A had the largest number of indicator species (10 species; Fig. 7a). Five of these taxa with IndVal indices of 1.00 were found exclusively in this cluster. The most abundant morphotype was *Umbellapathes* sp. with 33 records and a relative abundance within the cluster of 22.3%. *E. rostrata* was the most abundant taxa in Cluster B but, it also had a high relative abundance in clusters C, D, and F (Fig. 6b), and the pattern analysis associated *E. rostrata* with these four clusters as well. IndVal indices for morphotypes associated with cluster B were comparatively low (<0.53) with other clusters (Fig. 7b). Clusters C and D had a single species associated with them, *Sarostegia oculata* and *Gracilechinus* sp. respectively, which were the most abundant species for these clusters (Fig. 7c and d). Cluster E had four associated taxa whereas cluster F had two, all of them with IndVal indices above 0.82, except Aste6. In both clusters, species with the highest abundance were the ones with the highest IndVal indices (Fig. 7e and f).

The clusters showed distinct diversity characteristics and a trade-off between abundance and evenness (Table 3). Cluster A had the highest richness, Shannon index, and evenness across all clusters. Clusters C and F were characterized by a high abundance and richness, but a low evenness, which was primarily caused by the extreme dominance of *Sarostegia oculata* and *Aphanostichopathes* sp. In contrast, clusters B and E showed high evenness and low abundance and cluster D had an overall low abundance, Shannon index, and evenness. Segments in all clusters, except D, had a high dominance of VMEs indicator taxa. There was also a trade-off between sponges and corals dominance in clusters A, B, C, and F.

3.3. Environmental drivers

The variables rugosity and temperature were initially removed from further analysis due to high correlation (>0.7) with other variables. The PERMANOVA test identified four environmental variables that significantly explain some structure within the community data. The most noticeable were the factor variables Habitat ($R^2 = 0.347$, $p < 0.001$) and Region ($R^2 = 0.215$, $p < 0.001$), which together explained 56% of the variance in the data. Linear variables explained a much lower fraction of the variance, which only depth ($R^2 = 0.036$, $p < 0.001$) and slope ($R^2 = 0.009$, $p = 0.021$) of significance. The model had 35% of unexplained variance. The PERMDISP2 test showed no evidence of divergent dispersions for habitat ($F = 8.114$, $p < 0.001$) and region ($F = 7.929$, $p < 0.001$).

The nMDS ordination analysis supported the identified community clusters (Fig. 8a). The six clusters were separated from each other along the two axes and there was a small overlap in the confidence ellipses, more noticeably between clusters C and D. The nMDS plot showed a partial differentiation of segments based on habitat (Fig. 8b). It was possible to discern groups of segments with the same habitat, although some overlapping occurred between them. There was a pattern where segments of the same habitat were split into two clumps and amidst them is the habitat centroid (where the lines from all points converge). Each clump of the same habitat was associated with distinct regions (Fig. 8c), as the case for CalPav, CrSed, CrPav, and Sed. The segments obtained in the Northeast, Southwest, and the Center/South showed clear segregation between them in the nMDS plot (Fig. 8c), except for segments found in RiftCr habitat on both sides of the rift. Additionally, the segments obtained in the Center and South regions almost completely overlapped each other.

The Krustal-Wallis test indicated a significant difference in depth ($x^2 = 121.1$, $p < 0.001$) and slope ($x^2 = 96.6$, $p < 0.001$) in at least one cluster. Cluster A was the deepest one followed by cluster B, with a depth range from 1050 to 1250 m (Fig. 8d). Cluster E was the shallowest one, occurring above 700 m. Clusters C, D, and F were located mostly between 700 and 900 m, with no significant difference among them. Clusters A and B occurred in steeper areas than clusters D, E, and F (Fig. 8e). Cluster C was composed of segments in a wide slope extent, ranging from 0° to 70°. Cluster E had a significantly lower slope than others, with segments mostly occurring in flat areas.

The MRT analysis gave a seven-leaf tree with the splits based on region, habitat, depth, and slope (Fig. 9). The tree explained 58.6% of the Hellinger transformed morphotypes variance. Community structure varied strongly across the seven groups and displayed large contrasts in the multivariate mean of the most dominant morphotypes. The first split (Fig. 9) divided segments between Center/South and Northeast/Southwest regions. Segments in the Center/South regions were further split

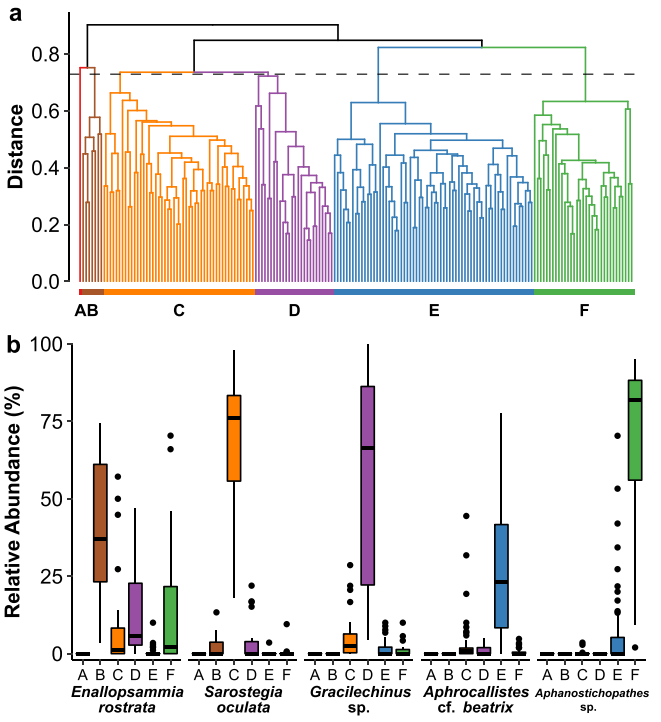

Fig. 6. (a) Dendrogram of the UPGMA clustering using Bray-Curtis dissimilarities of the log-transformed abundance of the segments. The dashed line indicates the height where the dendrogram was cut to create six clusters, labeled from A to F. **(b)** Boxplot of relative abundances in each cluster of the five most abundant taxa observed by *HyBIS* in Rio Grande Rise (SW Atlantic). The horizontal line through the box is the median and the lower and upper hinges correspond to the first and third quartiles, respectively. Upper and lower whiskers extend to the largest and smallest values, respectively, no further than 1.5 × interquartile range (IQR). Values beyond the end of the whiskers are plotted individually as points.

based on habitat. The habitat CalPav formed a node with a high abundance of *Gracilechinus* sp., and the other habitats were further split based on depth at 1077 m. The deeper node was dominated by *Enallopsammia rostrata* and the shallower one by *Sarostegia oculata*. A similar split at this depth range is visible in Fig. 8d, between cluster B and C. Region Southwest was split from Northeast and formed a node dominated by *Aphanostichopathes* sp. The Northeast region was further divided based on slope at 16.13° and steeper segments were also dominated by *S. oculata*. The other segments were in more flat areas (<16.13°) and were split into two nodes, based on habitat, and both had a high abundance of *Aphrocallistes* cf. *beatrix*. One node was formed by Cr and CrCob habitats, found uniquely at dive HY32, above and below the terrace in the northeast plateau, and showed a high abundance of a sponge classified as Corallistidae. The other node, in contrast, had a high abundance of another black coral, *Stichopathes* sp. (Anti2).

4. Discussion

Clear differences in megabenthic abundance were observed between the thirteen dives in the study area, which vary considerably in different spatial scales, ranging from nearly deserted bottoms to sponge gardens. The dives and Digital Terrain Model (DTM) exhibited highly heterogeneous habitats in RGR at different spatial scales (from meters to kilometers), changing rapidly from habitat to habitat. The community structure reflects the heterogeneous features of the RGR and it was strongly associated with habitat type and geographical regions of the study area. Similar patterns were observed by Perez et al. (2018) in the benthopelagic megafauna (restricted to fishes and crustaceans) outside of the study area. The fauna of RGR shows a high dominance of a few morphotypes, with *Sarostegia oculata* and *Aphanostichopathes* sp. each being 3.5 times more abundant than any other morphotype found. Hajdu et al. (2017) described a similar dominance of *S. oculata* at the rift wall and plateaus. In addition, species accumulation curves and richness estimators in our study did not reach asymptotes, indicating that longer dives in each habitat might be necessary to representatively quantify and assess megafauna diversity.

The PERMANOVA analysis suggests that seafloor characteristics (habitat type, depth, and slope) and geographic location were potential drivers of community structure, a result similar to comparable studies in Fe–Mn deposits areas in the Pacific Ocean (Delavenne et al., 2019; Morgan et al., 2015; Schlacher et al., 2014). The small area in our study revealed a wide range of habitats and potentially more could be found in RGR as an outcome of its complex topographic features, complex geological history, and associated environmental processes (Alberoni et al., 2020; Montserrat et al., 2019). Consistent with general patterns in the deep sea (Levin et al., 2001; Rex and Etter, 2010), our observations show that a high beta diversity was reflected by high habitat heterogeneity.

Habitats covered with Fe–Mn crusts (RiftCr, CrPav, Cr, CrSed, and CrCob) had more than one distinct community compared with other hard substrates, grouped in clusters C and E, and were rarely observed in other habitats. Likewise, Morgan et al. (2015) found evidence of changeover in diversity and community structure within cobalt-rich crusts areas and Schlacher et al. (2014) suggested the cover of cobalt-rich deposits may drive the structure of benthic communities. Polymetallic nodules in the Clarion-Clipperton Zone (CCZ) are also a potential driver for megafaunal community structure (Cuvelier et al., 2020; Durden et al., 2021; Simon-Lledó et al., 2020). Nevertheless, the exact relationship between the fauna and the chemical nature of the crusts and nodules remains to be further investigated. Based on microbial functional predictions performed in the study area, nitrification (i.e., ammonia oxidation and nitrite oxidation) and carbon fixation might be the main processes occurring in the Fe–Mn substrates by microbial communities (Bergo et al., 2021; Millo et al., 2022; Kfouri et al., 2021). The ecological roles microorganisms play in Fe–Mn crusts benthic ecosystems and in fauna colonization remains unknown (Orcutt et al., 2020), but they could be important contributors to the ecological process occurring in Fe–Mn crusts.

Geographic location (here factorized in four regions) explained more than one-fifth of the community structure. Removing Region from the PERMANOVA analysis reduced the model explained variation in 12.3% by other environmental variables. Region is likely a proxy for unmeasured parameters along the study area, including food availability, sedimentation, and bottom currents, or more complicated interactions between environmental variables. These parameters may drive drastic changes in communities (Levin et al., 2001) and account for differences between the Northeast, Center/South, and Southwest regions. Currents around RGR are strong (up to 50 cm/s) but variable due to tidal effects (Harlamov et al., 2015). The horizontal current velocity at the seabed is enhanced along with the shallower areas of the RGR summit plateaus (Montserrat et al., 2019) and the collected crusts show signs of erosion, indicating strong currents (Benites et al., 2020), as well as ripple marks found in soft sediment (this work). Currents are known to drive sponge species distribution on seamounts (Ramiro-Sánchez et al., 2019) and a fine circulation model in RGR could elucidate the effects of currents in the benthic fauna. The complex outlines of the rift wall and terraces possibly generate vortices and resuspensions favoring higher or lower food supply in specific areas. Moreover, the rift floor had a large amount of sediments and scarce hard substrate for sessile fauna. Suspension feeders, especially corals and sponges, are sensitive to high sediment loads (Morgan et al., 2015), which may account for the lower number of benthic fauna in this habitat.

The other two significant environmental drivers were depth and slope, albeit they explained only 4% of the variance. The lower rift wall

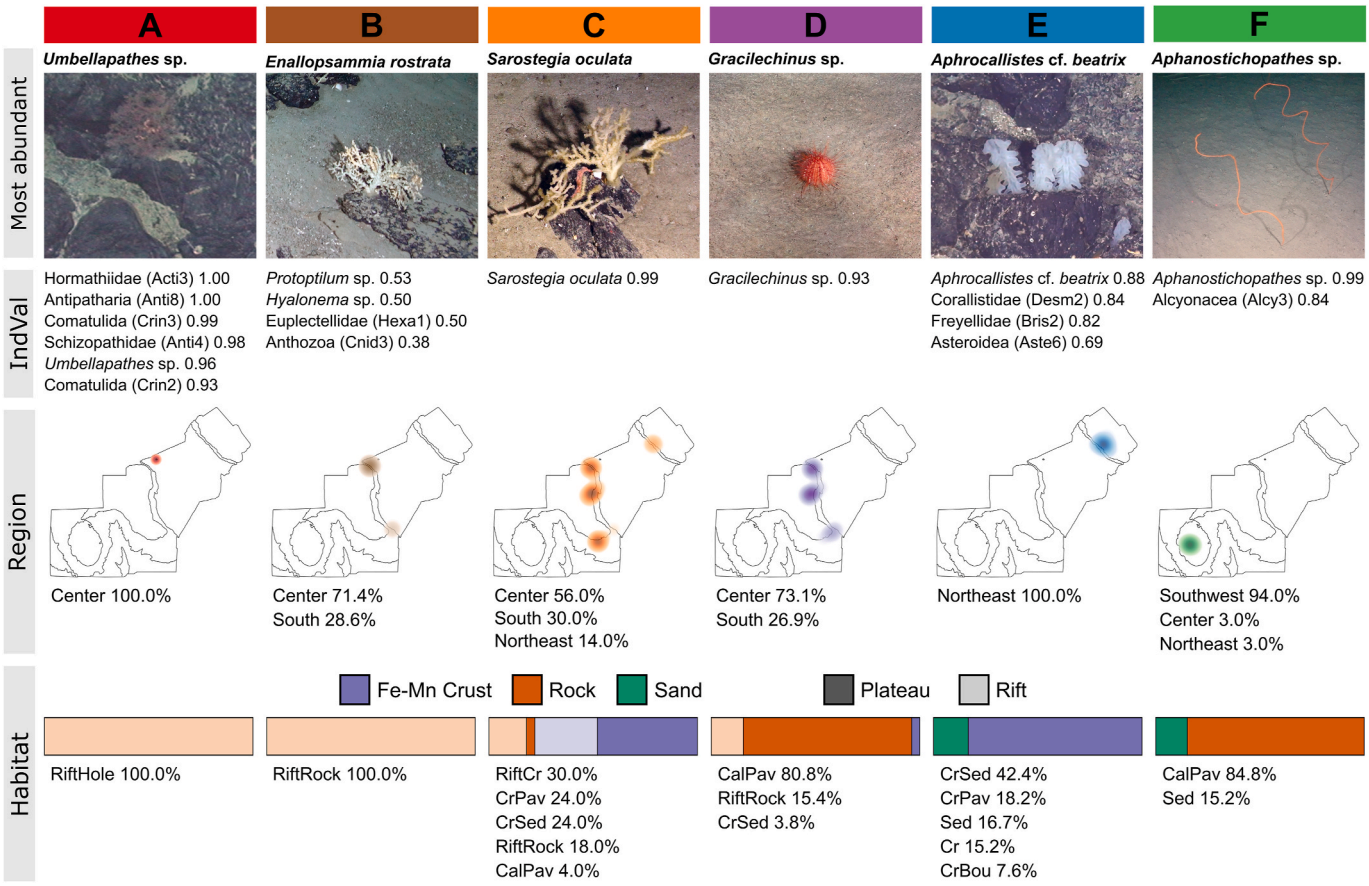

Fig. 7. Diagram summarizing key features of each cluster (columns), which corresponds to letters a-f in figure citations. **First row** shows photos of the most abundant morphotypes found in each cluster. They are from left to right: *Umbellapathes* sp, *Enallopsammia rostrata*, *Sarostegia oculata*, *Gracilechinus* sp., *Aphrocallistes* cf. *beatrix,* and *Aphanostichopathes* sp. **Second row** shows taxa associated with each cluster with $p < 0.05$ in the multilevel pattern analysis using IndVal as a function with a correction for clusters with different sizes. Values next to the taxa names are their respective IndVal indices. Note that for cluster A we omitted four morphotypes that had three or fewer records (Chry2, 1.00; Crin4, 1.00; Isid5, 1.00; and Desm3, 0.95). **Third row** shows a schematic map of the study area with locations where each cluster was detected and the percentage of segments for each region. **Fourth row** shows horizontal bars with the relative number of segments based on the type of substrate and whether the segment was located in the plateaus or the rift. Below is the percent of segments for each habitat. Fe–Mn crusts substrate includes RiftCr, CrSed, CrPav, Cr, and CrCob habitats; Rock includes RiftHole, RiftRock, and CalPav; and Sediment includes RiftSed and Sed habitats.

Table 3
Summary of the characteristics of the identified segment clusters. Values are reported as average ± standard deviation, except for Cluster A, as it has only one segment. The total richness is reported as general information and should not be directly compared between clusters due to the different segment numbers. VME - Vulnerable Marine Ecosystem.

Cluster		A	B	C	D	E	F
Number of segments		1	7	50	26	66	33
Abundance		148	42.29 ± 17.0	122.78 ± 93.0	52.54 ± 24.2	47.92 ± 28.7	153.55 ± 109.6
Average Richness (S)		18	8.57 ± 2.9	9.50 ± 2.8	7.19 ± 3.1	10.42 ± 2.8	10.12 ± 2.8
Total Richness		18	23	61	38	44	42
Shannon index (H′)		2.32	1.57 ± 0.48	1.04 ± 0.47	1.12 ± 0.65	1.74 ± 0.39	0.91 ± 0.45
Pielou's Evenness (J)		0.8	0.74 ± 0.15	0.47 ± 0.20	0.55 ± 0.24	0.75 ± 0.13	0.40 ± 0.19
VME indicators (% abundance)	**Sponges**	1.4	5.5 ± 4.3	75.9 ± 16.6	11.4 ± 18.3	48.4 ± 23.3	2.9 ± 5.9
	Corals	87.8	86.4 ± 4.3	11.7 ± 14.3	19.4 ± 19.8	32.9 ± 24.0	88.3 ± 14.6

was characterized by the cluster B communities in the RiftRock habitat, but the upper rift wall was marked by RiftCr and RiftRock habitats which accommodate communities grouped in cluster C. This shows that depth had a stronger effect on fauna composition than habitat at the rift wall, at roughly 1050 m depth near the transition from UCDW to AAIW. Water masses are known to have a significant influence on the distribution and composition of coral communities in the Southeast Brazilian continental slope (Arantes et al., 2009; Cavalcanti et al., 2017; Sumida et al., 2004), due to their distinct properties in the water column (temperature, salinity, oxygen, nutrients). In addition, microbial communities from pelagic zones in RGR are structured by water masses (Ferreira et al., 2021). Studies had shown that hexactinellids have high assimilation-to-respiration efficiency for bacteria (Bart et al., 2020), and they are an important functional group that links the pelagic microbial food web to the benthos (Pile and Young, 2006). Thus, our results suggest that water masses could explain some patterns observed in benthic fauna distribution, especially at distinct depths.

Other linear variables did not explain significant variance in the model, although they are proxies for habitat classification (Walbridge et al., 2018, and references therein) and are known to influence the

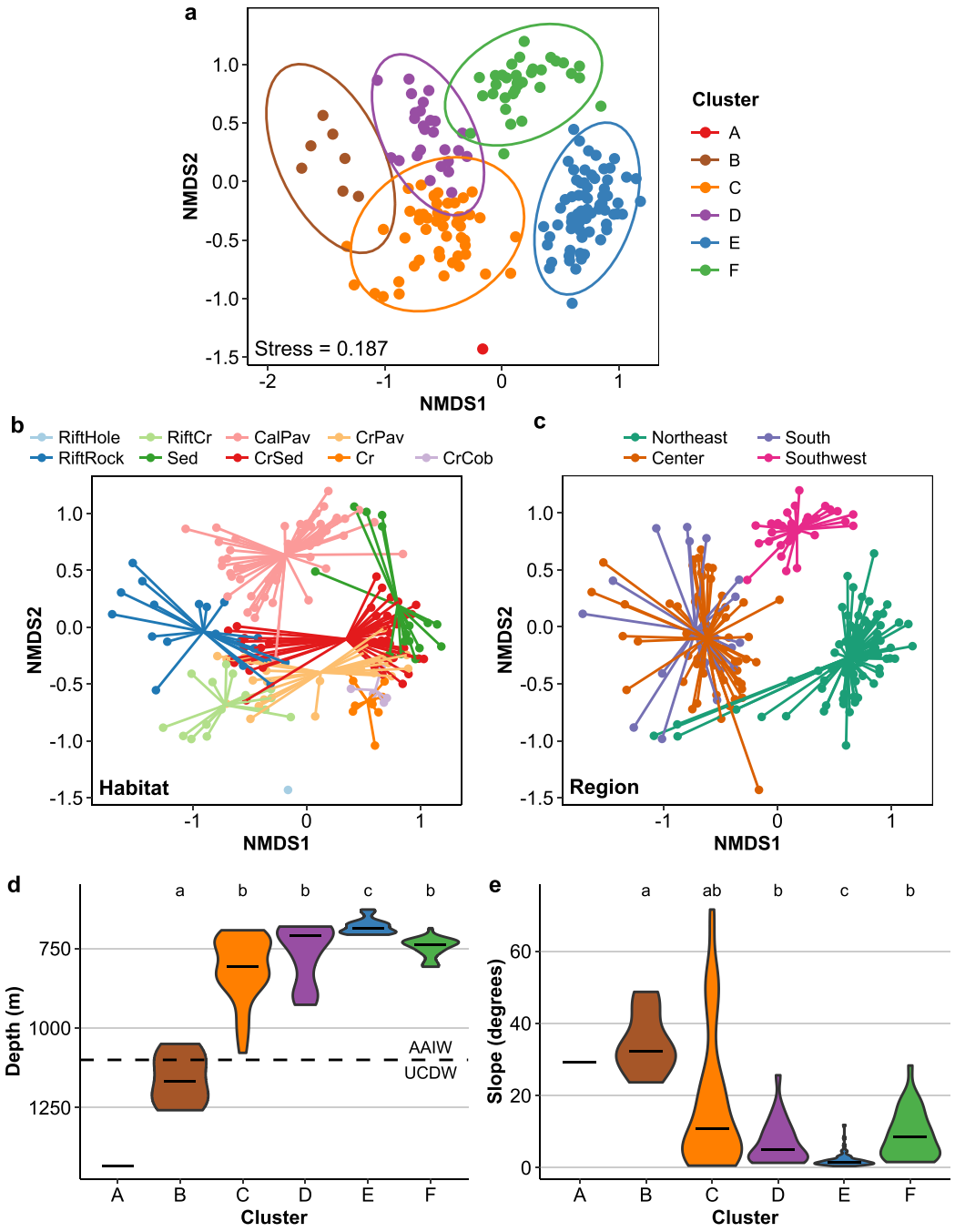

Fig. 8. **(a)** non-metric Multidimensional Scaling (nMDS) of the log-transformed abundance data using Bray-Curtis dissimilarities and two axes. Points are segments with 95% confidence ellipses and the colors represent different clusters. **(b–e)** All environmental variables selected by the PERMANOVA test with terms added sequentially. **(b, c)** Same nMDS as (a), but colors represent different habitats (b) and regions (c). Each point is connected to its group centroid. **(d, e)** Violin plots of depth (d) and slope (e). The letters above indicate the post-hoc Kruskal-Wallis comparison. Groups with the same letter are not significantly different. Cluster A was excluded from this analysis because it has only one segment. Dashed lines in (d) correspond to the transition between water masses. AAIW - Antarctic Intermediate Water and UCDW - Upper Circumpolar Deep Water.

abundance and distribution of species (e.g. García-Alegre et al., 2014; Morgan et al., 2015; Ramiro-Sánchez et al., 2019; Schlacher et al., 2014; Simon-Lledó et al., 2019). RGR is a complex structure, and the resolution of 15 m may not be sufficiently detailed to reveal small features (e.g. scarps, boulders) that are located within one grid cell and abrupt changes in slope that are found in the rift wall. Similarly, the sampling area in our study was limited and a broader geographic range could help to identify other environmental variables that drive the abundance and fauna composition in RGR.

The seamount megabenthic fauna tends to be dominated by suspension feeders, especially in deep-sea ecosystems (Rogers, 2018). Currents are accelerated by kilometer-scale topographic features, such as the rims or crests of seamount summits or ridges (Genin et al., 1989; Rogers, 2018), which increase food availability in these regions. The same patterns were observed in RGR, with the dominance of suspension feeders (*Sarostegia oculata*, *Aphanostichopathes* sp., *Enallopsammia rostrata,* and *Aphrocallistes* cf. *beatrix*) and evidence of strong currents (as discussed above). Topology and habitat are also known to drive deep-sea

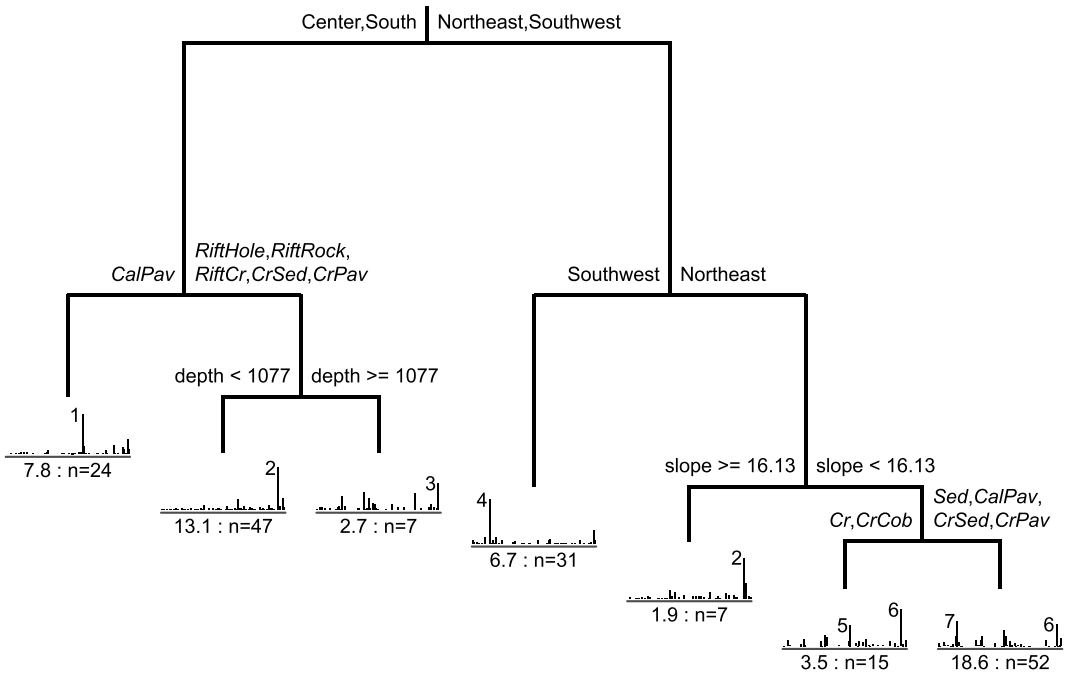

Fig. 9. Multivariate regression tree for Hellinger transformed abundance data. Relative error: 0.414, CVRE: 0.474, and CVRE standard error: 0.0262. Euclidean distance was used for splitting. Barplots show the multivariate morphotype mean at each node. Under barplots, the first value is the sum of squared errors and n is the number of sites in the leaf. Habitats are in italics; regions, in normal font; depth, in meters; and slope, in degrees. The morphotypes with the largest means are indicated with numbers next to their respective bars. 1 - *Gracilechinus* sp. (Echi2), 2 - *Sarostegia oculata* (Scep1), 3 - *Enallopsammia rostrata* (Scle1), 4 – *Aphanostichopathes* sp. (Anti1), 5 - Corallistidae (Desm2), 6 - *Aphrocallistes* cf. b*eatrix* (Scep2), 7 - *Stichopathes* sp. (Anti2).

communities in seamounts (Davies et al., 2015; Guinotte and Davies, 2014; Victorero et al., 2018). At first insights, patterns in benthic fauna of RGR are comparable to some trends found in other seamounts (but see discussion below). Despite these similarities, closed circulations above seamounts and internal wave formation may act to trap or provide a mechanism for the downward transport of phytoplankton and particulate organic carbon (POC) (Read and Pollard, 2017; Turnewitsch et al., 2016; Vilas et al., 2009; White et al., 2007). However, RGR is in the oligotrophic South Atlantic Gyre, with a low concentration of organic carbon (Perez et al., 2012) and the main reservoir of new nutrients is trapped below the permanent thermocline, in the South Atlantic Central Water (Ferreira et al., 2021). Physical processes induced by RGR and their biological consequences are unknown and should be investigated in future studies to ascertain which processes are related to the ones driven by seamounts.

4.1. Implications for conservation

The exploitation of Fe–Mn crusts will likely lead to loss of biological diversity resulting from direct habitat destruction, reduction in habitat heterogeneity, and changes in the geochemical characteristics of seafloor sediments (Christiansen et al., 2020; Levin et al., 2016). Indirect impacts on surrounding benthic and pelagic environments are possible through toxic and particle-rich sediment plumes, noise, vibration, and light created by the mining activity (Dunn et al., 2018; Jones et al., 2020; Miller et al., 2018). This sediment plume may cause smothering and burying of animals, clogging of feeding structures, and prevent larval settlement and colonization. Effects of particle load and toxicity could take years to decades to become visible (Weaver et al., 2022). We detected a diverse and rapidly-changing habitat in Rio Grande Rise, associated with evidence of strong currents and unique communities in Fe–Mn deposits. Thus, an extensive physical and biological analysis should occur prior to deep-sea areas being considered for exploitation in order to account for all areas that may be affected by mining activities.

Understanding spatial variations in megafaunal community structure, and their correlations with environmental parameters is crucial to predict and manage the environmental impacts of mining (Amon et al., 2016). *A priori* PERMANOVA model using only the linear variables (including latitude and longitude) had 56% of unexplained variance (a difference of 21.7% from our final model), suggesting that important environmental variables for community structure were not measured. Parameters like chemical properties of the water column, current velocity, and finer bathymetric and backscatter data may provide a better understanding of what is driving community structure in RGR and better predict regions of high diversity or unique fauna composition. The MRT analysis can present a comprehensive view of species-environment relationships, and aid contractors and governmental agencies to make better policies and management plans.

The study area contained many gardens of Vulnerable Marine Ecosystems (VMEs) indicator species, including sponges and corals. Such species are characterized as long-lived, late-maturing, slow-growing, with low larval recruitment, and dispersal potential (Ardron et al., 2014). VMEs have low resilience and slow recovery from human disturbances such as bottom-contact fishing and, in the future, deep-sea mining. Benites et al. (2020) concluded that bulk RGR crusts in the study area are enriched in Ni and Li, which are critical metals of economic interest. Some crusts and substrate rocks had high P, F, and carbonate fluorapatite (CFA) contents (Benites et al., 2020) and might be considered potential phosphate ores in deep-sea mining. *Sarostegia oculata* and *Aphrocallistes* cf. *beatrix* are examples of dominant VMEs indicator species with a high affinity for Fe–Mn crusts, which were not found in other habitats. Criteria used to identify VMEs are often based on benthic bycatch during fishing operations (Auster et al., 2011) and only recently density thresholds were used to objectively identify VMEs (Long et al., 2020; Rowden et al., 2020). For example, Rowden et al. (2020) applied thresholds of 0.11–0.85 coral head m^{-2} of *Solenosmilia variabilis*. If we roughly consider that our videos cover 5-m wide area, we would find a maximum density of 0.71 individuals m^{-2} of *S. oculata* and

28 out of 183 segments would have a density higher than 0.11, which suggests that some areas of RGR could in fact constitute VMEs. Comprehensive studies should address the potential impacts in these communities before and during mining operations.

Assessing similarities between benthic communities from the RGR and adjacent areas in the South Atlantic is a key factor in order to assert the extent of impacts in RGR to other regions, such as the Jean Charcot Seamounts, Vitória-Trindade seamounts chain, Southeast Brazilian continental margin, Mid-Atlantic Ridge and the 'sister' Walvis Ridge. The framework-forming *Solenosmilia variabilis* and *Desmophyllum pertusum* (former *Lophelia pertusa*) were the most dominant cold-water scleractinians in the Brazilian continental slope (Cavalcanti et al., 2017; Pires, 2007). Both corals were not recorded in our study, which suggests that communities are different in both regions. Differences in invertebrate assemblages between the Vitória-Trindade seamount chain and the Brazilian continental shelf has been recorded before (O'Hara et al., 2010), but only for above 150 m depth. In addition, *S. oculata* and *Aphrocallistes* cf. *beatrix* are recorded in the Vitória-Trindade seamounts chain (Tabachnick et al., 2009) and *E. rostrata* is distributed off Southeast Brazil continental margin (Arantes et al., 2009; Kitahara et al., 2020). Addressing the connectivity between populations of RGR and the South Atlantic is another important element highly relevant in the context of future mineral exploration (Perez et al., 2018).

Sampling techniques using video and still imagery vary across studies by using different sampling units. Some may use photographs or a collection of photographs (Durden et al., 2021), running length (this work, Perez et al., 2018), or dives (Morgan et al., 2015; Schlacher et al., 2014). Density, richness, and diversity can be difficult to relate across these studies. When possible, the area is often calculated from photos and video images to facilitate the comparison of megafaunal data across deep-sea studies (e.g. Amon et al., 2016; Cuvelier et al., 2020; Durden et al., 2021; Simon-Lledó et al., 2019). However, RGR is a complex feature with many steep slopes and rough terrain, which would represent a strong bias in the surface estimations in some habitats. The current development and dissemination of 3D photogrammetry (Bayley et al., 2019; Lim et al., 2020; Price et al., 2021) may prove useful tools to better estimate the area and density on such topologies, and compare results across other surveys.

The limited collection of voucher specimens in our study precludes robust assessments of endemicity due to limitations of identifying organisms to species level using videos. Lima et al. (2019) recorded nine species of antipatharians in the RGR, and only one was shared with the Brazilian continental margin. Such result was only possible due to physical sampling of biological specimens and precise taxonomic identifications. In addition, a study by Delavenne et al. (2019) revealed that Fe–Mn crusts at French Polynesia EEZ are inhabited by distinct macrobenthic communities. This result would not be possible using submarine imaging techniques alone. It is critical that future studies combine imagery data with physical collection of specimens to obtain reliable estimates of species richness and species ranges (Amon et al., 2016).

5. Conclusions

RGR is a large and heterogeneous feature with abrupt and common changes in habitat, where little is known about its biodiversity and ecological patterns so far. Although the area studied here is very small compared to the whole RGR, our results indicate clear spatial patterns in faunal composition that are influenced by habitats and the presence Fe–Mn crusts. We discussed a set of environmental drivers, both abiotic and biotic, that may be influencing the distribution and abundance of species, but more studies with a broader geological scale are needed to unfold what drives the community structure and to understand its ecological patterns. The life history and morphological traits of the fauna observed imply that any recovery from mining is likely to be very slow, thus affected and surrounding areas must be considered in order to implement a strategic environmental management plan and help to address biodiversity conservation in the future. RGR has heterogeneous habitats that may require more complex regulations that treat each habitat as multiple ecological units.

Declaration of competing interest

The authors declare that they have no known competing financial interests or personal relationships that could have appeared to influence the work reported in this paper.

Acknowledgments

This study was funded by the Fundação de Amparo a Pesquisa do Estado de São Paulo (FAPESP, BR) grant number 2014/50820-7 and the Natural Environment Research Council (NERC, UK), as part of the Brazil-UK joint project "Marine ferromanganese deposits: a major resource of E-tech elements". PVFC was funded by FAPESP grant number 2017/11884-8 and PYGS was funded by CNPq grant number 301554/2019-6. We are grateful to the Captain and Crew Members of the N/Oc. Alpha Crucis and *RSS Discovery* for their professionalism and dedication to data acquisition. We thank Cristiana Castello-Branco (Smithsonian Institution), Eduardo Hajdu (Museu Nacional - UFRJ), Marcelo Kitahara (UNIFESP), Jose Angel Alvarez Perez (CTTMar - UNIVALI), Sérgio Nascimento Stampar (UNESP - FCL/Assis) and Renata Carolina Mikosz Arantes (UFSC) for their invaluable help to identify the fauna observed on the videos.

Appendix A. Supplementary data

Supplementary data to this article can be found online at https://doi.org/10.1016/j.dsr.2022.103811.

References

Alberoni, A.A.L., Jeck, I.K., Silva, C.G., Torres, L.C., 2020. The new Digital Terrain Model (DTM) of the Brazilian Continental Margin: detailed morphology and revised undersea feature names. Geo Mar. Lett. 40, 949–964. https://doi.org/10.1007/s00367-019-00606-x.

Amon, D.J., Ziegler, A.F., Dahlgren, T.G., Glover, A.G., Goineau, A., Gooday, A.J., Wiklund, H., Smith, C.R., 2016. Insights into the abundance and diversity of abyssal megafauna in a polymetallic-nodule region in the eastern Clarion-Clipperton Zone. Sci. Rep. 6, 30492 https://doi.org/10.1038/srep30492.

Anderson, M.J., 2001. A new method for non-parametric multivariate analysis of variance: non-parametric manova for ecology. Austral Ecol. 26, 32–46. https://doi.org/10.1111/j.1442-9993.2001.01070.

Anderson, M.J., 2006. Distance-based tests for homogeneity of multivariate dispersions. Biometrics 62, 245–253.

Arantes, R., Castro, C., Pires, D., Seoane, J., 2009. Depth and water mass zonation and species associations of cold-water octocoral and stony coral communities in the southwestern Atlantic. Mar. Ecol. Prog. Ser. 397, 71–79. https://doi.org/10.3354/meps08230.

Ardron, J.A., Clark, M.R., Penney, A.J., Hourigan, T.F., Rowden, A.A., Dunstan, P.K., Watling, L., Shank, T.M., Tracey, D.M., Dunn, M.R., Parker, S.J., 2014. A systematic approach towards the identification and protection of vulnerable marine ecosystems. Mar. Pol. 49, 146–154. https://doi.org/10.1016/j.marpol.2013.11.017.

Auster, P.J., Gjerde, K., Heupel, E., Watling, L., Grehan, A., Rogers, A.D., 2011. Definition and detection of vulnerable marine ecosystems on the high seas: problems with the "move-on" rule. ICES J. Mar. Sci. 68, 254–264. https://doi.org/10.1093/icesjms/fsq074.

Baker, P.F., 1983. Tectonic evolution and subsidence history of the Rio Grande rise. In: Initial Reports of the Deep Sea Drilling Project. US Government Printing Office, Washington, DC, pp. 953–976.

Baker, E., Beaudoin, Y., 2013. Cobalt-rich Ferromanganese Crusts: A Physical, Biological, Environmental, and Technical Review. Secretariat of the Pacific Community.

Bart, M.C., de Kluijver, A., Hoetjes, S., Absalah, S., Mueller, B., Kenchington, E., Rapp, H. T., de Goeij, J.M., 2020. Differential processing of dissolved and particulate organic matter by deep-sea sponges and their microbial symbionts. Sci. Rep. 10, 17515 https://doi.org/10.1038/s41598-020-74670-0.

Bayley, D.T.I., Mogg, A.O.M., Koldewey, H., Purvis, A., 2019. Capturing complexity: field-testing the use of 'structure from motion' derived virtual models to replicate standard measures of reef physical structure. PeerJ 7, e6540. https://doi.org/10.7717/peerj.6540.

Benites, M., Hein, J.R., Mizell, K., Blackburn, T., Jovane, L., 2020. Genesis and evolution of ferromanganese crusts from the summit of Rio Grande rise, Southwest Atlantic ocean. Minerals 10, 349. https://doi.org/10.3390/min10040349.

Benites, M., Hein, J.R., Mizell, K., Jovane, L., 2021. Miocene phosphatization of rocks from the summit of Rio Grande rise, Southwest Atlantic ocean. Paleoceanogr. Paleoclimatol. 36, e2020PA004197 https://doi.org/10.1029/2020PA004197.

Bergo, N.M., Bendia, A.G., Ferreira, J.C.N., Murton, B.J., Brandini, F.P., Pellizari, V.H., 2021. Microbial diversity of deep-sea ferromanganese crust field in the Rio Grande rise, southwestern atlantic ocean. Microb. Ecol. https://doi.org/10.1007/s00248-020-01670-y.

Borcard, D., Gillet, F., Legendre, P., 2018. Numerical Ecology with R, second ed. Use R! Springer International Publishing, Cham, Switzerland. https://doi.org/10.1007/978-3-319-71404-2.

Cáceres, M.D., Legendre, P., 2009. Associations between species and groups of sites: indices and statistical inference. Ecology 90, 3566–3574. https://doi.org/10.1890/08-1823.1.

Cavalcanti, J.A.D., Santos, R.V., Lacasse, C.M., Rojas, J.N.L., Nobrega, M., 2015. Potential mineral resources of phosphates and trace elements on the Rio Grande rise, South Atlantic ocean. In: 44th Underw. Min. Conf..

Caruso, J.H., 1989. Systematics and distribution of Atlantic chaunacid anglerfishes (Pisces: Lophiiformes). Copeia 1, 153–165.

Cavalcanti, G. de H., Arantes, R.C.M., Falcão, A.P. da C., Curbelo-Fernandez, M.P., Silveira, M.A. da S., Politano, A.T., Viana, A.R., Hercos, C.M., Brasil, A.C., dos, S., 2017. Ecossistemas de corais de águas profundas da Bacia de Campos. In: Comunidades Demersais e Bioconstrutores. Elsevier, Rio de Janeiro, pp. 43–85. https://doi.org/10.1016/B978-85-352-7295-6.50003-8.

Christiansen, B., Denda, A., Christiansen, S., 2020. Potential effects of deep seabed mining on pelagic and benthopelagic biota. Mar. Policy, Environmental governance of deep seabed mining - scientific insights and food for thought 114, 103442. https://doi.org/10.1016/j.marpol.2019.02.014.

Clark, M.R., Vinnichenko, V.I., Gordon, J.D.M., Beck-Bulat, G.Z., Kukharev, N.N., Kakora, A.F., 2007. Large-scale distant-water trawl fisheries on seamounts. In: Seamounts: Ecology, Fisheries & Conservation. Blackwell Publishing Ltd, Oxford, UK, pp. 361–399. https://doi.org/10.1002/9780470691953.ch17.

Constantino, R.R., Hackspacher, P.C., de Souza, I.A., Lima Costa, I.S., 2017. Basement structures over Rio Grande rise from gravity inversion. J. South Am. Earth Sci. 75, 85–91. https://doi.org/10.1016/j.jsames.2017.02.005.

Core Team, R., 2020. R: A Language and Environment for Statistical Computing. R Foundation for Statistical Computing, Vienna, Austria.

Cuvelier, D., Ribeiro, P.A., Ramalho, S.P., Kersken, D., Martinez Arbizu, P., Colaço, A., 2020. Are seamounts refuge areas for fauna from polymetallic nodule fields? Biogeosciences 17, 2657–2680. https://doi.org/10.5194/bg-17-2657-2020.

da Silveira, I.C.A., Napolitano, D.C., Farias, I.U., 2020. Water masses and oceanic circulation of the Brazilian continental margin and adjacent abyssal plain. In: Sumida, P.Y.G., Bernardino, A.F., De Léo, F.C. (Eds.), Brazilian Deep-Sea Biodiversity, Brazilian Marine Biodiversity. Springer International Publishing, Cham, pp. 7–36. https://doi.org/10.1007/978-3-030-53222-2_2.

Davies, J.S., Stewart, H.A., Narayanaswamy, B.E., Jacobs, C., Spicer, J., Golding, N., Howell, K.L., 2015. Benthic assemblages of the anton dohrn seamount (NE atlantic): defining deep-sea biotopes to support habitat mapping and management efforts with a focus on vulnerable marine ecosystems. PLoS One 10, e0124815. https://doi.org/10.1371/journal.pone.0124815.

Delavenne, J., Keszler, L., Castelin, M., Lozouet, P., Maestrati, P., Samadi, S., 2019. Deep-sea benthic communities in the largest oceanic desert are structured by the presence of polymetallic crust. Sci. Rep. 9, 6977. https://doi.org/10.1038/s41598-019-43325-0.

De'ath, G., 2002. Multivariate regression trees: a new technique for modeling species-environment relationships. Ecology 83, 1105. https://doi.org/10.2307/3071917.

Dufrêne, M., Legendre, P., 1997. Species Assemblages and Indicator Species: the need for a flexible asymmetrical approach. Ecol. Monogr. 67, 345–366. https://doi.org/10.1890/0012-9615(1997)067[0345:SAAIST]2.0.CO;2.

Dunn, D.C., Dover, C.L.V., Etter, R.J., Smith, C.R., Levin, L.A., Morato, T., Colaço, A., Dale, A.C., Gebruk, A.V., Gjerde, K.M., Halpin, P.N., Howell, K.L., Johnson, D., Perez, J.A.A., Ribeiro, M.C., Stuckas, H., Weaver, P., Participants, S.W., 2018. A strategy for the conservation of biodiversity on mid-ocean ridges from deep-sea mining. Sci. Adv. 4, eaar4313. https://doi.org/10.1126/sciadv.aar4313.

Durden, J.M., Putts, M., Bingo, S., Leitner, A.B., Drazen, J.C., Gooday, A.J., Jones, D.O. B., Sweetman, A.K., Washburn, T.W., Smith, C.R., 2021. Megafaunal ecology of the western clarion clipperton zone. Front. Mar. Sci. 8, 671062 https://doi.org/10.3389/fmars.2021.671062.

Ferreira, J.C.N., Bergo, N.M., Tura, P.M., Chuqui, M.G., Brandini, F.P., Jovane, L., Pellizari, V.H., 2021. Abundance and microbial diversity from surface to deep water layers over the Rio Grande rise, South Atlantic (preprint). Microbiology. https://doi.org/10.1101/2021.04.22.441028.

García-Alegre, A., Sánchez, F., Gómez-Ballesteros, M., Hinz, H., Serrano, A., Parra, S., 2014. Modelling and mapping the local distribution of representative species on the le danois bank, el cachucho marine protected area (cantabrian sea). Deep sea res. Part II top. Stud. Oceanogr. Oceanogr. Bay Biscay 106, 151–164. https://doi.org/10.1016/j.dsr2.2013.12.012.

Genin, A., Noble, M., Lonsdale, P.F., 1989. Tidal currents and anticyclonic motions on two North Pacific seamounts. Deep-Sea Res. Part A Oceanogr. Res. Pap. 36, 1803–1815. https://doi.org/10.1016/0198-0149(89)90113-1.

Glover, A.G., Smith, C.R., 2003. The deep-sea floor ecosystem: current status and prospects of anthropogenic change by the year 2025. Environ. Conserv. 30, 219–241. https://doi.org/10.1017/S0376892903000225.

Graça, M.C., Kusznir, N., Gomes Stanton, N.S., 2019. Crustal thickness mapping of the central South Atlantic and the geodynamic development of the Rio Grande rise and Walvis Ridge. Mar. Petrol. Geol. 101, 230–242. https://doi.org/10.1016/j.marpetgeo.2018.12.011.

Gräler, B., Pebesma, E., Heuvelink, G., 2016. Spatio-Temporal Interpolation using gstat. R J 8, 204–218.

Greene, H.G., Yoklavich, M.M., Starr, R.M., O'Connell, V.M., Wakefield, W.W., Sullivan, D.E., McRea, J.E., Cailliet, G.M., 1999. A classification scheme for deep seafloor habitats. Oceanol. Acta 22, 663–678. https://doi.org/10.1016/S0399-1784(00)88957-4.

Gray, J.E., 1858. On *Aphrocallistes*, a New Genus of Spongiadae from Malacca. Proc. Zool. Soc. London 26, 114–115.

Greene, H.G., Bizzarro, J.J., O'Connell, V.M., Brylinsky, C.K., 2007. Construction of Digital Potential Marine Benthic Habitat Maps Using a Coded Classification Scheme and its Application 16.

Guilhon, M., Montserrat, F., Turra, A., 2021. Recognition of ecosystem-based management principles in key documents of the seabed mining regime: implications and further recommendations. ICES J. Mar. Sci. 78, 884–899. https://doi.org/10.1093/icesjms/fsaa229.

Guinotte, J.M., Davies, A.J., 2014. Predicted deep-sea coral habitat suitability for the U. S. West coast. PLoS One 9, e93918. https://doi.org/10.1371/journal.pone.0093918.

Hajdu, E., Castello-Branco, C., Lopes, D.A., Sumida, P.Y.G., Perez, J.A.A., 2017. Deep-sea dives reveal an unexpected hexactinellid sponge garden on the Rio Grande Rise (SW Atlantic). A mimicking habitat? Deep Sea Res. Part II Top. Stud. Oceanogr. 146, 93–100. https://doi.org/10.1016/j.dsr2.2017.11.009.

Harlamov, V., Lisniowski, M., Frazao, E., Pessoa, J., Aguiar, R., Lopes, V., Nobrega, M., Lisboa, M., Simoes, H., Cavalacanti, J., Pessanha, I., 2015. Preliminary results onmid-depth circulation features on Rio Grande Rise. In: 2015 IEEE/OES Acoustics in Underwater Geosciences Symposium (RIO Acoustics). Presented at the 2015 IEEE/OES Acoustics in Underwater Geosciences Symposium (RIO Acoustics). IEEE, Rio de Janeiro, pp. 1–8. https://doi.org/10.1109/RIOAcoustics.2015.7473647.

Hein, J.R., Koschinsky, A., 2014. Deep-ocean ferromanganese crusts and nodules. In: Treatise on Geochemistry. Elsevier, pp. 273–291. https://doi.org/10.1016/B978-0-08-095975-7.01111-6.

Herzig, P.M., Hannington, M.D., 1995. Polymetallic massive sulfides at the modern seafloor A review. Ore Geol. Rev. 10, 95–115. https://doi.org/10.1016/0169-1368(95)00009-7.

Hughes, D.J., Shimmield, T.M., Black, K.D., Howe, J.A., 2015. Ecological impacts of large-scale disposal of mining waste in the deep sea. Sci. Rep. 5, 9985. https://doi.org/10.1038/srep09985.

ISA, 2014. Decision of the Council relating to an application for the approval of a plan of work for exploration for cobalt-rich ferromanganese crusts by Companhia de Pesquisa de Recursos Minerais. ISBA/20/C/30. Int. Seabed Auth. [WWW Document] http://www.isa.org.jm/files/documents/EN/20Sess/Council/ISBA-20C-30.pdf. (Accessed 21 February 2017).

Jones, D.O.B., Ardron, J.A., Colaço, A., Durden, J.M., 2020. Environmental considerations for impact and preservation reference zones for deep-sea polymetallic nodule mining. Mar. Pol. 118 https://doi.org/10.1016/j.marpol.2018.10.025.

Jovane, L., Hein, J.R., Yeo, I.A., Benites, M., Bergo, N.M., Corrêa, P.V.F., Couto, D.M., Guimarães, A.D., Howarth, S.A., Miguel, H.R., Mizell, K.L., Moura, D.S., Vicentini Neto, F.L., Pompeu, M., Rodrigues, I.M.M., Santana, F.R., Serrao, P.F., Silva, T.E., Tura, P.M., Viscarra, C.L., Chuqui, M.G., Pellizari, V.H., Signori, C.N., Da Silveira, I. C.A., Sumida, P.Y.G., Murton, B.J., Brandini, F.P., 2019. Multidisciplinary scientific cruise to the Rio Grande rise. Front. Mar. Sci. 6, 252. https://doi.org/10.3389/fmars.2019.00252.

Kfouri, L.O., Millo, C., de Lima, A.E., Silveira, C.S., Sant'Anna, L.G., Marino, E., González, F.J., Sayeg, I.J., Hein, J.R., Jovane, L., Bernardini, S., Lusty, P.A.J., Murton, B.J., 2021. Growth of ferromanganese crusts on bioturbated soft substrate, Tropic Seamount, northeast Atlantic ocean. Deep-Sea Res. Part A Oceanogr. Res. Pap. 175, 103586 https://doi.org/10.1016/j.dsr.2021.103586.

Kitahara, M.V., Cordeiro, R.T.S., Barbosa, R.V., Pires, D. de Oliveira, Sumida, P.Y.G., 2020. Brazilian deep-sea corals. In: Sumida, P.Y.G., Bernardino, A.F., De Léo, F.C. (Eds.), Brazilian Deep-Sea Biodiversity, Brazilian Marine Biodiversity. Springer International Publishing, Cham, pp. 73–107. https://doi.org/10.1007/978-3-030-53222-2_4.

Kruskal, W.H., Wallis, W.A., 1952. Use of ranks in one-criterion variance analysis. J. Am. Stat. Assoc. 47, 583–621. https://doi.org/10.1080/01621459.1952.10483441.

LEPLAC, 2018. Executive summary: Brazilian partial revised submission to the commission on the limits of the continental shelf [WWW Document]. Braz. Cont. Shelf Surv. Program. URL. https://www.un.org/depts/los/clcs_new/submissions_files/bra02_rev18/BR-OMM-ExecutiveSummary.pdf. (Accessed 2 January 2021).

Levin, L.A., Etter, R.J., Rex, M.A., Gooday, A.J., Smith, C.R., Pineda, J., Stuart, C.T., Hessler, R.R., Pawson, D., 2001. Environmental influences on regional deep-sea species diversity. Annu. Rev. Ecol. Systemat. 32, 51–93. https://doi.org/10.1146/annurev.ecolsys.32.081501.114002.

Levin, L.A., Mengerink, K., Gjerde, K.M., Rowden, A.A., Van Dover, C.L., Clark, M.R., Ramirez-Llodra, E., Currie, B., Smith, C.R., Sato, K.N., Gallo, N., Sweetman, A.K., Lily, H., Armstrong, C.W., Brider, J., 2016. Defining "serious harm" to the marine environment in the context of deep-seabed mining. Mar. Pol. 74, 245–259. https://doi.org/10.1016/j.marpol.2016.09.032.

Lim, A., Wheeler, A.J., Price, D.M., O'Reilly, L., Harris, K., Conti, L., 2020. Influence of benthic currents on cold-water coral habitats: a combined benthic monitoring and 3D photogrammetric investigation. Sci. Rep. 10, 19433 https://doi.org/10.1038/s41598-020-76446-y.

Lima, M.M., Cordeiro, R.T.S., Perez, C.D., 2019. Black corals (anthozoa: antipatharia) from the southwestern atlantic. Zootaxa 4692, 1–67. https://doi.org/10.11646/zootaxa.4692.1.1.

Long, S., Sparrow-Scinocca, B., Blicher, M.E., Hammeken Arboe, N., Fuhrmann, M., Kemp, K.M., Nygaard, R., Zinglersen, K., Yesson, C., 2020. Identification of a soft

coral garden candidate vulnerable marine ecosystem (VME) using video imagery, davis strait, west Greenland. Front. Mar. Sci. 7.
Magurran, A.E., 2004. Measuring Biological Diversity. Blackwell Publishing, Oxford.
Manceau, A., Lanson, M., Takahashi, Y., 2014. Mineralogy and crystal chemistry of Mn, Fe, Co, Ni, and Cu in a deep-sea Pacific polymetallic nodule. Am. Mineral. 99, 2068–2083. https://doi.org/10.2138/am-2014-4742.
McArdle, B.H., Anderson, M.J., 2001. Fitting multivariate models to community data: a comment on distance-based redundancy analysis. Ecology 82, 290–297. https://doi.org/10.1890/0012-9658(2001)082[0290:FMMTCD]2.0.CO;2.
McClain, C.R., Hardy, S.M., 2010. The dynamics of biogeographic ranges in the deep sea. Proc. R. Soc. B Biol. Sci. 277, 3533–3546. https://doi.org/10.1098/rspb.2010.1057.
Miller, K.A., Thompson, K.F., Johnston, P., Santillo, D., 2018. An overview of seabed mining including the current state of development, environmental impacts, and knowledge gaps. Front. Mar. Sci. 4, 418. https://doi.org/10.3389/fmars.2017.00418.
Millo, C., Vieira do Nascimento e Silva, M.H., de Mello, R.M., Leckie, R.M., Benites, M., Fonseca Giannini, P.C., Boggiani, P.C., Bosence, D., Lusty, P.A.J., Murton, B.J., Jovane, L., 2022. Discovery of enigmatic toroidal carbonate concretions on the Rio Grande rise (southwestern atlantic ocean). Mar. Geol. 443, 106665 https://doi.org/10.1016/j.margeo.2021.106665.
Mohriak, W., 2020. Genesis and evolution of the South Atlantic volcanic islands offshore Brazil. Geo Mar. Lett. 40, 1–33. https://doi.org/10.1007/s00367-019-00631-w.
Mohriak, W.U., Nobrega, M., Odegard, M.E., Gomes, B.S., Dickson, W.G., 2010. Geological and geophysical interpretation of the Rio Grande Rise, south-eastern Brazilian margin: extensional tectonics and rifting of continental and oceanic crusts. Petrol. Geosci. 16, 231–245. https://doi.org/10.1144/1354-079309-910.
Montserrat, F., Guilhon, M., Corrêa, P.V.F., Bergo, N.M., Signori, C.N., Tura, P.M., Santos Maly, M. de los, Moura, D., Jovane, L., Pellizari, V., Sumida, P.Y.G., Brandini, F.P., Turra, A., 2019. Deep-sea mining on the Rio Grande Rise (Southwestern Atlantic): a review on environmental baseline, ecosystem services and potential impacts. Deep-Sea Res. Part A Oceanogr. Res. Pap. 145, 31–58. https://doi.org/10.1016/j.dsr.2018.12.007.
Mora, C., Tittensor, D.P., Adl, S., Simpson, A.G.B., Worm, B., 2011. How many species are there on earth and in the ocean? PLoS Biol. 9, e1001127 https://doi.org/10.1371/journal.pbio.1001127.
Morato, T., Cleary, J., Taranto, G.H., Bilan, M., Barros, I., Vandeperre, F., Pham, C.K., Dunn, D.C., Colaço, A., Halpin, P.N., 2016. In: Data Report: towards Development of a Strategic Environmental Management Plan for Deep Seabed Mineral Exploitation in the Atlantic Basin. IMAR & MGEL, Horta, Portugal. https://www.eu-midas.net/sites/default/files/Workshops/SEMPIA/SEMPIA_Data_Report_lowres.pdf. (Accessed 28 August 2017).
Morgan, N.B., Cairns, S., Reiswig, H., Baco, A.R., 2015. Benthic megafaunal community structure of cobalt-rich manganese crusts on Necker Ridge. Deep-Sea Res. Part A Oceanogr. Res. Pap. 104, 92–105. https://doi.org/10.1016/j.dsr.2015.07.003.
Mourato, B.L., Arfelli, C.A., Amorim, A.F., Hazin, H.G., Carvalho, F.C., Hazin, F.H.V., 2011. Spatio-temporal distribution and target species in a longline fishery off the southeastern coast of Brazil. Braz. J. Oceanogr. 59, 185–194. https://doi.org/10.1590/S1679-87592011000200007.
Murton, B.J., Huhnerbach, V., Garrard, J., 2012. HyBIS: a new concept in versatile, 6000-m rated robotic underwater vehicles. In: Roberts, G.N., Sutton, R. (Eds.), Further Advances in Unmanned Marine Vehicles. Institution of Engineering and Technology, pp. 45–67. https://doi.org/10.1049/PBCE077E_ch3.
Oksanen, J., Blanchet, F.G., Friendly, M., Kindt, R., Legendre, P., McGlinn, D., Minchin, P.R., O'Hara, R.B., Simpson, G.L., Solymos, P., Stevens, M.H.H., Szoecs, E., Wagner, H., 2019. Vegan: Community Ecology Package.
Orcutt, B.N., Bradley, J.A., Brazelton, W.J., Estes, E.R., Goordial, J.M., Huber, J.A., Jones, R.M., Mahmoudi, N., Marlow, J.J., Murdock, S., Pachiadaki, M., 2020. Impacts of deep-sea mining on microbial ecosystem services. Limnol. Oceanogr. 65, 1489–1510. https://doi.org/10.1002/lno.11403.
O'Connor, J.M., Duncan, R.A., 1990. Evolution of the Walvis Ridge-Rio Grande Rise Hot Spot Systen : Implications for African and South American Plate Motions over Plumes.
O'Hara, T.D., Consalvey, M., Lavrado, H.P., Stocks, K.I., 2010. Environmental predictors and turnover of biota along a seamount chain: assemblage composition along a seamount chain. Mar. Ecol. 31, 84–94. https://doi.org/10.1111/j.1439-0485.2010.00379.x.
Perez, J., dos Santos Alves, E., Clark, M., Bergstad, O.A., Gebruk, A., Azevedo Cardoso, I., Rogacheva, A., 2012. Patterns of life on the southern mid-Atlantic Ridge: compiling what is known and addressing future Research. Oceanography 25, 16–31. https://doi.org/10.5670/oceanog.2012.102.
Perez, J.A.A., Kitazato, H., Sumida, P.Y.G., Sant'Ana, R., Mastella, A.M., 2018. Benthopelagic megafauna assemblages of the Rio Grande rise (SW atlantic). Deep-Sea Res. Part A Oceanogr. Res. Pap. 134, 1–11. https://doi.org/10.1016/j.dsr.2018.03.001.
Peterson, R.G., Whitworth, T., 1989. The subantarctic and polar fronts in relation to deep water masses through the southwestern Atlantic. J. Geophys. Res. 94, 10817 https://doi.org/10.1029/JC094iC08p10817.
Pielou, E.C., 1966. The measurement of diversity in different types of biological collections. J. Theor. Biol. 13, 131–144. https://doi.org/10.1016/0022-5193(66)90013-0.
Pile, A.J., Young, C.M., 2006. The natural diet of a hexactinellid sponge: benthic–pelagic coupling in a deep-sea microbial food web. Deep-Sea Res. Part A Oceanogr. Res. Pap. 53, 1148–1156. https://doi.org/10.1016/j.dsr.2006.03.008.
Pires, D. de O., 2007. The azooxanthellate coral fauna of Brazil. Bull. Mar. Sci. 81, 265–272.
Pourtalès, L.F., 1878. Corals. In: Reports on the dredging operations of the U.S. Coast Survey Steamer "Blake". Bulletin of the Museum of Comparative Zoology at Harvard College, in Cambridge 5, 197–212.
Price, D.M., Lim, A., Callaway, A., Eichhorn, M.P., Wheeler, A.J., Lo Iacono, C., Huvenne, V.A.I., 2021. Fine-scale heterogeneity of a cold-water coral reef and its influence on the distribution of associated taxa. Front. Mar. Sci. 8 https://doi.org/10.3389/fmars.2021.556313.
Ramirez-Llodra, E., Brandt, A., Danovaro, R., De Mol, B., Escobar, E., German, C.R., Levin, L.A., Martinez Arbizu, P., Menot, L., Buhl-Mortensen, P., Narayanaswamy, B. E., Smith, C.R., Tittensor, D.P., Tyler, P.A., Vanreusel, A., Vecchione, M., 2010. Deep, diverse and definitely different: unique attributes of the world's largest ecosystem. Biogeosciences 7, 2851–2899. https://doi.org/10.5194/bg-7-2851-2010.
Ramiro-Sánchez, B., González-Irusta, J.M., Henry, L.-A., Cleland, J., Yeo, I., Xavier, J.R., Carreiro-Silva, M., Sampaio, Í., Spearman, J., Victorero, L., Messing, C.G., Kazanidis, G., Roberts, J.M., Murton, B., 2019. Characterization and mapping of a deep-sea sponge ground on the tropic seamount (northeast tropical atlantic): implications for spatial management in the high seas. Front. Mar. Sci. 6 https://doi.org/10.3389/fmars.2019.00278.
Read, J., Pollard, R., 2017. An introduction to the physical oceanography of six seamounts in the southwest Indian Ocean. Deep Sea Res. Part II Top. Stud. Oceanogr. Pelagic Ecol. Seamounts South West Indian Ocean 136, 44–58. https://doi.org/10.1016/j.dsr2.2015.06.022.
Rex, M.A., Etter, R.J., 2010. Deep-sea Biodiversity: Pattern and Scale. Harvard University Press, Cambridge, Mass.
Rogers, A.D., 2018. Chapter four - the biology of seamounts: 25 Years on. In: Sheppard, C. (Ed.), Advances in Marine Biology. Academic Press, pp. 137–224. https://doi.org/10.1016/bs.amb.2018.06.001.
Rowden, A.A., Pearman, T.R.R., Bowden, D.A., Anderson, O.F., Clark, M.R., 2020. Determining coral density thresholds for identifying structurally complex vulnerable marine ecosystems in the deep sea. Front. Mar. Sci. 7, 95. https://doi.org/10.3389/fmars.2020.00095.
Schlacher, T.A., Baco, A.R., Rowden, A.A., O'Hara, T.D., Clark, M.R., Kelley, C., Dower, J.F., 2014. Seamount benthos in a cobalt-rich crust region of the central Pacific: conservation challenges for future seabed mining. Divers. Distrib. 20, 491–502. https://doi.org/10.1111/ddi.12142.
Simon-Lledó, E., Bett, B.J., Huvenne, V.A.I., Schoening, T., Benoist, N.M.A., Jeffreys, R. M., Durden, J.M., Jones, D.O.B., 2019. Megafaunal variation in the abyssal landscape of the clarion clipperton zone. Prog. Oceanogr. 170, 119–133. https://doi.org/10.1016/j.pocean.2018.11.003.
Simon-Lledó, E., Pomee, C., Ahokava, A., Drazen, J.C., Leitner, A.B., Flynn, A., Parianos, J., Jones, D.O.B., 2020. Multi-scale variations in invertebrate and fish megafauna in the mid-eastern Clarion Clipperton Zone. Prog. Oceanogr. 187, 102405 https://doi.org/10.1016/j.pocean.2020.102405.
Stramma, L., England, M., 1999. On the water masses and mean circulation of the South Atlantic Ocean. J. Geophys. Res. Oceans 104, 20863–20883. https://doi.org/10.1029/1999JC900139.
Sumida, P.Y.G., Yoshinaga, M.Y., Madureira, L.A.S.-P., Hovland, M., 2004. Seabed pockmarks associated with deepwater corals off SE Brazilian continental slope. Santos Basin. Mar. Geol. 207, 159–167. https://doi.org/10.1016/j.margeo.2004.03.006.
Tabachnick, K.R., Menshenina, L.L., Lopes, D.A., Hajdu, E., 2009. Two new *Hyalonema* species (Hyalonematidae: amphidiscosida) from eastern and south-eastern Brazil, and further Hexactinellida (Porifera) collected from seamounts off south-eastern Brazil by the RV 'Marion Dufresne' MD55 expedition. J. Mar. Biol. Assoc. U. K. 89, 1243–1250. https://doi.org/10.1017/S0025315409000253.
Thompson, K.F., Miller, K.A., Currie, D., Johnston, P., Santillo, D., 2018. Seabed mining and approaches to governance of the deep seabed. Front. Mar. Sci. 5 https://doi.org/10.3389/fmars.2018.00480.
Thurber, A.R., Sweetman, A.K., Narayanaswamy, B.E., Jones, D.O.B., Ingels, J., Hansman, R.L., 2014. Ecosystem function and services provided by the deep sea. Biogeosciences 11, 3941–3963. https://doi.org/10.5194/bg-11-3941-2014.
Topsent, E., 1904. *Sarostegia oculata*, Hexactinellide nouvelle des îles du Cap-Vert. Bull. du Musée Océanographique de Monaco 10, 1–8.
Turnewitsch, R., Dumont, M., Kiriakoulakis, K., Legg, S., Mohn, C., Peine, F., Wolff, G., 2016. Tidal influence on particulate organic carbon export fluxes around a tall seamount. Prog. Oceanogr. 149, 189–213. https://doi.org/10.1016/j.pocean.2016.10.009.
Ussami, N., Chaves, C.A.M., Marques, L.S., Ernesto, M., 2013. Origin of the Rio Grande Rise-Walvis Ridge reviewed integrating palaeogeographic reconstruction, isotope geochemistry and flexural modelling. Geol. Soc. Lond. Spec. Publ. 369, 129–146. https://doi.org/10.1144/SP369.10.
Van Dover, C.L., Ardron, J.A., Escobar, E., Gianni, M., Gjerde, K.M., Jaeckel, A., Jones, D. O.B., Levin, L.A., Niner, H.J., Pendleton, L., Smith, C.R., Thiele, T., Turner, P.J., Watling, L., Weaver, P.P.E., 2017. Biodiversity loss from deep-sea mining. Nat. Geosci. 10, 464–465. https://doi.org/10.1038/ngeo2983.
Victorero, L., Robert, K., Robinson, L.F., Taylor, M.L., Huvenne, V.A.I., 2018. Species replacement dominates megabenthos beta diversity in a remote seamount setting. Sci. Rep. 8, 4152. https://doi.org/10.1038/s41598-018-22296-8.
Vilas, J.C., Arístegui, J., Kiriakoulakis, K., Wolff, G.A., Espino, M., Polo, I., Montero, M. F., Mendonça, A., 2009. Seamounts and organic matter—is there an effect? The case of Sedlo and Seine Seamounts: Part 1. Distributions of dissolved and particulate organic matter. Deep Sea Res. Part II Top. Stud. Oceanogr. 56, 2618–2630. https://doi.org/10.1016/j.dsr2.2008.12.023.
Walbridge, S., Slocum, N., Pobuda, Marjean, Wright, D., 2018. Unified geomorphological analysis workflows with benthic terrain modeler. Geosciences 8, 94. https://doi.org/10.3390/geosciences8030094.

Weaver, P.P.E., Aguzzi, J., Boschen-Rose, R.E., Colaço, A., de Stigter, H., Gollner, S., Haeckel, M., Hauton, C., Helmons, R., Jones, D.O.B., Lily, H., Mestre, N.C., Mohn, C., Thomsen, L., 2022. Assessing plume impacts caused by polymetallic nodule mining vehicles. Mar. Pol. 139, 105011 https://doi.org/10.1016/j.marpol.2022.105011.

Wedding, L.M., Friedlander, A.M., Kittinger, J.N., Watling, L., Gaines, S.D., Bennett, M., Hardy, S.M., Smith, C.R., 2013. From principles to practice: a spatial approach to systematic conservation planning in the deep sea. Proc. R. Soc. B Biol. Sci. 280, 20131684. https://doi.org/10.1098/rspb.2013.1684, 20131684.

White, M., Bashmachnikov, I., Arístegui, J., Martins, A., 2007. Physical processes and seamount productivity. In: Seamounts: Ecology, Fisheries & Conservation. John Wiley & Sons, Ltd, pp. 62–84. https://doi.org/10.1002/9780470691953.ch4.

Wickham, H., 2016. ggplot2: Elegant Graphics for Data Analysis. Springer-Verlag, New York.